



Atmospheric oxidation of α,β -unsaturated ketones: kinetics and mechanism of the OH radical reaction

Niklas Illmann¹, Rodrigo Gastón Gibilisco², Justinian Gabriel Bejan³, Iulia Patroescu-Klotz¹, and Peter Wiesen¹

¹Institute for Atmospheric and Environmental Research, Bergische Universität Wuppertal, 42097 Wuppertal, Germany

²INQUINOA-UNT-CONICET Institute of Physical Chemistry, Faculty of Biochemistry, Chemistry and Pharmacy, National University of Tucumán, San Lorenzo 456, T4000CAN, San Miguel de Tucumán, Argentina

³Faculty of Chemistry and Integrated Centre of Environmental Science Studies in the North Eastern Region Alexandru Ioan Cuza University of Iasi, 11 Carol I, Iasi 700506, Romania

Correspondence: Niklas Illmann (illmann@uni-wuppertal.de)

Received: 28 May 2021 – Discussion started: 11 June 2021

Revised: 31 July 2021 – Accepted: 3 August 2021 – Published: 14 September 2021

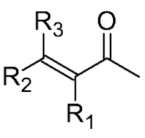
Abstract. The OH-radical-initiated oxidation of 3-methyl-3-penten-2-one and 4-methyl-3-penten-2-one was investigated in two atmospheric simulation chambers at 298 ± 3 K and 990 ± 15 mbar using long-path FTIR spectroscopy. The rate coefficients of the reactions of 3-methyl-3-penten-2-one and 4-methyl-3-penten-2-one with OH radicals were determined to be $(6.5 \pm 1.2) \times 10^{-11}$ and $(8.1 \pm 1.3) \times 10^{-11}$ cm³ molecule⁻¹ s⁻¹, respectively. To enlarge the kinetics data pool the rate coefficients of the target species with Cl atoms were determined to be $(2.8 \pm 0.4) \times 10^{-10}$ and $(3.1 \pm 0.4) \times 10^{-10}$ cm³ molecule⁻¹ s⁻¹, respectively. The mechanistic investigation of the OH-initiated oxidation focuses on the RO₂+NO reaction. The quantified products were acetoin, acetaldehyde, biacetyl, CO₂ and peroxyacetyl nitrate (PAN) for the reaction of 3-methyl-3-penten-2-one with OH radicals and acetone, methyl glyoxal, 2-hydroxy-2-methylpropanal, CO₂ and peroxyacetyl nitrate (PAN) for the reaction of 4-methyl-3-penten-2-one with OH, respectively. Based on the calculated product yields an upper limit of 0.15 was determined for the yield of RONO₂ derived from the OH reaction of 4-methyl-3-penten-2-one. By contrast, no RONO₂ formation was observed for the OH reaction of 3-methyl-3-penten-2-one. Additionally, a simple model is presented to correct product yields for secondary processes.

1 Introduction

The α,β -unsaturated ketones are a particular class of oxygenated volatile organic compounds (OVOCs) emitted either from biogenic and/or anthropogenic sources or generated in the oxidation of airborne VOCs in the atmosphere. The most prominent representative among this class is methyl vinyl ketone (MVK). MVK is, on the one hand, emitted from the polymer, pharmaceutical and fungicide manufacturing industries (Siegel and Eggersdorfer, 2000). On the other hand, it is formed in the troposphere, mainly through the gas-phase oxidation of isoprene, the NMHC which is most abundantly emitted into the atmosphere, with an estimated annual emission up to 750 Tg (Calvert et al., 2000; Guenther et al., 2006). Other α,β -unsaturated ketones, like 3-methyl-3-penten-2-one (3M3P2), are used in the fragrances and food industry (Chapuis and Jacoby, 2001; Bickers et al., 2003, Wang et al., 2020). Furthermore, 4-methyl-3-penten-2-one (4M3P2), commonly known as mesityl oxide, is a precursor of methyl isobutyl ketone used extensively as solvent in the fabrication of paints and coatings. Production rates as high as 0.1 Tg yr⁻¹ were reported in the US (Sifniades et al., 2011). α,β -Unsaturated ketones were also identified in laboratory studies on emissions from different fuels representative of biomass burning (Hatch et al., 2017).

During daytime the main loss process of α,β -unsaturated ketones, once released into or formed in the atmosphere, is probably the oxidation initiated by OH radicals, which has a direct impact on the atmospheric ozone and secondary organic aerosol formation (Kanakidou et al., 2005; Calvert

Table 1. Structures of α,β -unsaturated ketones and related literature on the corresponding OH-radical-initiated oxidation mechanism.

Structure	R_1	R_2	R_3	Name	Reference
	–H	–H	–H	Methyl vinyl ketone (3-Buten-2-one)	Tuazon and Atkinson, (1989); Galloway et al. (2011); Praske et al. (2015); Fuchs et al. (2018)
	–H	–CH ₃	–H	3-Penten-2-one	Illmann et al. (2021b)
	–CH ₃	–H	–H	3-Methyl-3-buten-2-one	–
	–CH ₃	–CH ₃	–H	3-Methyl-3-penten-2-one	This work
	–H	–CH ₃	–CH ₃	4-Methyl-3-penten-2-one	Gaona-Colmán et al. (2017); This work

et al., 2011). However, our knowledge about the oxidation mechanisms of species presented in Table 1 is rather limited. To date, only the OH radical reaction of MVK has been intensively studied (Tuazon and Atkinson, 1989; Galloway et al., 2011; Praske et al., 2015; Fuchs et al., 2018). Under high-NO conditions, where virtually all peroxy radicals react with NO, glycolaldehyde and methyl glyoxal together with formaldehyde and PAN were identified as first-generation products. Praske et al. (2015) also found a low RONO₂ yield of about 4%. Some attention was also given to the reaction of both 3M3P2 and 4M3P2, investigated in the present study, with O₃ and to the 3M3P2+Cl and 3M3P2+NO₃ system (Sato et al., 2004; Canosa-Mas et al., 2005; Wang et al., 2015; Illmann et al., 2021a; Li et al., 2021). Gaona-Colmán et al. (2017) investigated the OH radical reaction of 4M3P2. However, they qualitatively identified only formaldehyde and acetone (GC-MS detection). Hence, the mechanism remains rather incomplete.

In this work, we present an in-depth investigation of the OH-radical-initiated oxidation of two di-substituted α,β -unsaturated ketones, namely 3M3P2 and 4M3P2. Besides the first determination of the rate coefficient for the reaction of OH radicals with 3M3P2, we report kinetic data for Cl atom reactions.

In order to correct the formation yields of products formed in target reactions within complex experimental systems it is quite common to use the Tuazon formalism (Tuazon et al., 1986). This is based on the assumption that reaction products are subsequently consumed in secondary processes like photolysis, wall loss and oxidation by OH radicals. Thus, their formation yields in the target reactions are underestimated when determined from plotting the formed product against the consumed compound of interest, and the yields increase when corrected. However, the formalism is difficult to apply for products with secondary sources in the reaction system. In this case, the formation yields are overestimated without proper corrections. For this purpose, we present a simple model to correct molar formation yields in the target reactions, which accounts for both consumption and secondary formation processes.

The study investigates the contribution of the OH-initiated oxidation of both 3M3P2 and 4M3P2 to the formation of

NO_x reservoir species, like peroxyacetyl nitrate (PAN), in the atmosphere. Apart for being an important NO_x reservoir species for the atmosphere, PAN is a phytotoxic air pollutant (Vyskocil et al., 1998) with sources that are still unaccounted for (Fischer et al., 2014). PAN formation depends strongly on temperature and the levels of NO₂ and NO. The study stresses the importance of determining either the ratio between PAN and CO₂/HCHO or the PAN yield together with the NO₂/NO ratio within the experiment since these give more comprehensive information on NO_x reservoir species production than the PAN yield alone. Therefore experiments were conducted under varying NO₂/NO ratios.

2 Experimental

Experiments were carried out in a 1080 and a 480 L reaction chamber in 990 ± 15 mbar of synthetic air at 298 ± 3 K. In the following section is given an updated description of both chambers. A major improvement of both chambers is the addition of heatable injection blocks (< 100 °C). A controlling unit allows the temperature to be adjusted for a better transfer of samples into the reaction chamber, according to the thermal stability of the investigated substances. Graphic representations of the chambers were published already by Barnes and co-workers (Barnes et al., 1993; Barnes et al., 1994).

2.1 1080 L chamber

The 1080 L chamber consists of two joint quartz-glass tubes with a total length of 6.2 m and an inner diameter of 0.47 m connected via a middle flange. It is closed at both ends by metal flanges bearing several ports for the injection of reactants, addition of bath gases and coupling with analytical devices. A total of 32 superactinic fluorescent lamps (Philips TL05 40 W: 300–460 nm, max. intensity at ca. 360 nm) and 32 low-pressure mercury vapour lamps (Philips TUV 40 W: max. intensity at 254 nm) can be used to irradiate the reaction mixture. These lamps are wired in parallel and spaced evenly around the reaction vessel. The pumping system consists of a turbo-molecular pump backed by a double-stage rotary fore pump. The chamber is cleaned between experiments by evac-

uating it to 10^{-4} mbar for at least 30 min. Cleanliness of the chamber is proved by FTIR. Homogeneity of the reaction mixtures is achieved by three magnetically coupled Teflon mixing fans, which are placed on the end and middle flanges. A White-type mirror system is installed inside the chamber to monitor reaction mixtures via FTIR spectroscopy in the spectral range $4000\text{--}700\text{ cm}^{-1}$ at a resolution of 1 cm^{-1} . The system whose base length is $(5.91 \pm 0.01)\text{ m}$ was operated at 82 traverses which yields a total optical path length of $(484.7 \pm 0.8)\text{ m}$. Spectra were recorded using a Nicolet iS50 instrument equipped with a liquid-nitrogen-cooled mercury-cadmium-telluride (MCT) detector.

The initial mixing ratios in the 1080 L experiments, in ppmV ($1\text{ ppmV} = 2.46 \times 10^{13}\text{ molecules cm}^{-3}$ at 298 K), were 0.7–1.3 for 3-methyl-3-penten-2-one (3M3P2), 0.9–1.8 for 4-methyl-3-penten-2-one (4M3P2), 1.1 for isoprene, 0.9–1.4 for propene, 0.9–1.4 for isobutene, 0.9–1.4 for 1,3-butadiene, 0.9–1.9 for methyl nitrite, 0.9–1.9 for Cl_2 , 2–4 for NO and 0–2.5 for NO_2 .

2.2 480 L chamber

The smaller chamber in the Wuppertal laboratory consists of a borosilicate glass cylinder with a total volume of 480 L (length of 3 m and 0.45 m inner diameter). The tube is closed at both ends by aluminium flanges containing various ports for the introduction of reactants and bath gases, sampling, and instruments monitoring the physical parameters inside the chamber. To ensure homogeneous mixing of the reactants a magnetically coupled fan is mounted on the front flange inside the chamber. A total of 32 fluorescent lamps (Philips TLA 40 W, $300 \leq \lambda \leq 460\text{ nm}$, I_{max} at 360 nm) are mounted in four boxes and spaced evenly around the chamber. The lamp housings are cooled with air and their inner surface is encased in reflective steel sheets. The lamps can be switched individually to allow a variation of the photolysis frequency and consequently the radical level during photolysis experiments. The pumping system consists of a rotary vane pump and a root pump yielding an end vacuum of up to 10^{-3} mbar. For a typical cleaning procedure between two experiments the chamber is completely evacuated and filled up to 200–300 mbar of synthetic air or nitrogen. This procedure is repeated until it is certain that no signals related to the previous experiment are detected. Reactants and products are monitored using in situ FTIR spectroscopy. For this purpose, a White-type mirror system (base length: $2.80 \pm 0.01\text{ m}$) is installed inside the chamber and coupled to a Nicolet 6700 FTIR spectrometer (MCT detector). The system is operated at 18 traverses, which yields a total optical path length of $50.4 \pm 0.2\text{ m}$. FTIR spectra are recorded in the spectral range $4000\text{--}700\text{ cm}^{-1}$ at a resolution of 1 cm^{-1} .

The initial mixing ratios in the 480 L experiments in ppmV ($1\text{ ppmV} = 2.46 \times 10^{13}\text{ molecules cm}^{-3}$ at 298 K) were 5.0–6.1 for 3-methyl-3-penten-2-one (3M3P2), 5.0–6.0 for 4-methyl-3-penten-2-one (4M3P2), 5.0–5.7 for methyl valer-

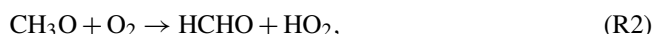
ate, 4.2–6.3 for propene, 4.2–6.3 for isobutene, 4.2–6.3 for 1,3-butadiene, 10–16 for methyl nitrite, 13–16 for Cl_2 and 20–27 for NO.

2.3 Materials

The following chemicals were used without further handling, with purities as stated by the suppliers: isobutene (Sigma Aldrich, 99%), propene (Air Liquide, 99.95%), 1,3-butadiene (Messer, > 99%), isoprene (Aldrich, 99%), methyl valerate (Alfa Aesar, 99%), 3-methyl-3-penten-2-one (Sigma Aldrich, tech. 90%), 4-methyl-3-penten-2-one (Sigma Aldrich, tech. 90%), acetoin (Sigma Aldrich, 96%), biacetyl (Sigma Aldrich, 97%), 2-methyl-3-buten-2-ol (Sigma Aldrich, 98%), carbon monoxide (Air Liquide, 99.97%), nitrogen monoxide (Air Liquide, 99.5%), nitrogen dioxide (Messer Griesheim, > 98%), Cl_2 (Air Liquide, 99.8%), synthetic air (Messer, 99.9999%), nitrogen (Messer, 99.9999%). Methyl nitrite was synthesized by dropping sulfuric acid in an ice-cooled aqueous solution of sodium nitrite and methanol (Taylor et al., 1980). The product was collected and stored in a cooling trap at $-78\text{ }^\circ\text{C}$. The purity of methyl nitrite was confirmed via FTIR spectroscopy.

2.4 Experimental protocol

OH radicals were generated by methyl nitrite photolysis in synthetic air at 360 nm:



NO was added to the reaction system to suppress ozone formation and hence the formation of NO_3 radicals. Cl atoms were generated by photolysis of molecular chlorine in either synthetic air or nitrogen at 360 nm:



In both chambers, the target compound and the products formed during the reaction (mechanistic investigation) as well as the target and reference compound (kinetic study experiments) were monitored using FTIR spectroscopy. Typically, 50–70 interferograms were co-added per spectrum, which results in averaging period of about 80–113 s, and 15–20 spectra were recorded per experiment. In each run the first five spectra were collected in the dark, over a period of 10–20 min, to check for a potential wall loss of the unsaturated ketones and the reference compounds. Afterwards, the reaction was started by switching on the lamps. In the product study experiments, the reaction was terminated after a maximum of 10 spectra were recorded. In selected experiments additionally 5 spectra were collected in the dark, after termination, over a time interval of 10–20 min, to investigate the significance of the wall loss for the products of the oxidation reaction in the experimental system.

Usually, the housing which enfolds the transfer optics between FTIR spectrometer and chamber is flushed with purified dry air. Therefore, quantification of CO₂ is, due to a slight variability in the dry air supply, unreliable under normal laboratory conditions. To be able to quantify CO₂, in selected product study experiments performed in the 1080 L chamber, the transfer optics housing was flushed with ultra-pure N₂ evaporated from a liquid nitrogen tank.

2.5 Relative rate method

The rate coefficients for the reaction of OH radicals and Cl atoms with the α,β -unsaturated ketones were determined by relating the consumption of the ketone to the consumption of at least two reference compounds:



Both ketones and references could potentially be subject to an irreversible first-order wall loss:



Considering these processes the following equation can be derived:

$$\begin{aligned} \ln\left(\frac{[\text{ketone}]_0}{[\text{ketone}]_t}\right) - k_{\text{loss,ketone}} \times t \\ = \frac{k_{\text{ketone}}}{k_{\text{ref.}}} \times \left(\ln\left(\frac{[\text{ref.}]_0}{[\text{ref.}]_t}\right) - k_{\text{loss,ref.}} \times t\right), \end{aligned} \quad (1)$$

where $[X]_t$ is the concentration of the species X at time t and $t = 0$ corresponds to the time where the lamps were switched on. According to Eq. (1) a plot of $\{\ln([\text{ketone}]_0/[\text{ketone}]_t) - k_{\text{loss,ketone}} \times t\}$ against $\{\ln([\text{ref.}]_0/[\text{ref.}]_t) - k_{\text{loss,ref.}} \times t\}$ should yield a straight line with zero intercept where the slope represents the rate coefficient ratio $k_{\text{ketone}}/k_{\text{ref.}}$.

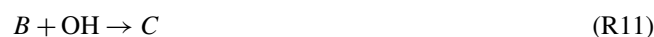
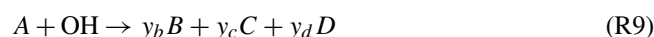
2.6 Product identification and quantification

The quantification of identified products was done by subtraction of calibrated reference IR spectra. The corresponding concentrations of the reference spectra were calculated based on cross sections either taken from literature references, taken from the Wuppertal laboratory's database or determined within this work. For methyl glyoxal we used the cross sections determined by Talukdar et al. (2011). When employing the values reported by Profeta et al. (2011) the obtained mixing ratios of methyl glyoxal are, however, almost identical. Peroxyacetyl nitrate (PAN) has been quantified using the absorption cross section reported by Allen et al. (2005). Cross sections for acetone and acetaldehyde were taken from the Wuppertal database. The absorption cross sections of 3-methyl-3-penten-2-one, 4-methyl-3-penten-2-one, 3-hydroxy-2-butanone (acetoin) and 2,3-butanedione

(biacetyl) were determined within this work by either injecting different volumes of the pure compound into the chamber, evaporating weighted solid samples (in the case of acetoin) into a flow of bath gas or injecting aliquot volumes of a solution containing the target species according to a method previously described by Etzkorn et al. (1999). Reference spectra of 2-hydroxy-2-methylpropanal (HMPr) were generated in situ by the ozonolysis of 2-methyl-3-buten-2-ol in the presence of CO to scavenge any OH radical formed in the reaction system. CO₂ was quantified by integration of the absorption features in the range 2400–2349 cm⁻¹ and a polynomial calibration function derived from the injection of various volumes of CO₂ using a calibrated gas-tight syringe.

2.7 Modelling

In order to correct the experimentally determined product yields for both secondary formation and consumption a simple model was established based on the Euler–Cauchy method, which can be written down using a commercially available calculation program. In doing so, the rates $d[X]/dt$ for each species X are calculated for constant time intervals Δt based on the rate equation and the concentration of the species X in the previous time interval. This allows the calculation of concentration changes for each time interval, which, when added to the concentration of the previous time interval, yield the concentration of X at time t . The model assumes simplified reaction mechanisms as exemplarily shown below.



The simplest version of this approach assumes a steady-state (sst) concentration of OH radicals that can be determined from the individual loss rate of the target species A during the irradiation period of each experiment. This hypothesis is valid as long as pseudo-first-order conditions are proven by a linear correlation between $\{\ln([A]_0/[A]_t) - k_{\text{wall}} \times t\}$ and the time t . The modelled concentration time profiles are obtained by the input of $[A]_0$, $[\text{OH}]_{\text{sst}}$ and the rate coefficients of all listed Reactions (R9)–(R14). The yield y_x for each product of the target reaction is included as a parameter to be varied until the simulated concentration–time profile of each species matches the experimental data. However, for traceability and potential future applications, we prefer to outline in detail the stepwise procedure which turned out as best practice after several tests.

1. The rate equations for each species are written according to the simplified exemplary mechanism shown

above in Reactions (R9)–(R14), where kinetic data and molar formation yields for the secondary reactions are taken from literature references. Values for the first-order rate coefficients of each species' wall loss are included if they are measured in the same experiment (thus measured before and after the irradiation of the reaction mixture). If they are not measured, values for k_{wall} are first set to zero and included as additional variables. Molar formation yields for the target reaction are included as variable y_x .

2. Time intervals Δt and the total duration t are adjusted and the initial concentration $[A]_0$ of A is included for $t = 0$ according to the experimental data.
3. If the experimental logarithmic decay of the concentration of A demonstrates pseudo-first-order conditions, a constant OH concentration is included based on the consumption of A during the irradiation. If pseudo-first-order conditions are not accomplished within the experiment the OH concentration has to be described as a function of t based on the consumption of A . However, including the OH concentration yields a simulated time profile for A which should reproduce the experimental data of A well.
4. Finally, the parameters y_x for the target reaction are varied until the time profile of each species matches the experimental data, starting with y_x corresponding to species X , which is the less affected by secondary reactions. Thus, one would start with y_d and y_b rather than y_c in the given example. The uncorrected molar yields y_x , derived from plotting the measured mixing ratio of product X against the consumed target species A , are appropriate as a starting point of the iterative process. If wall losses were not determined within the experiments one should try to match the time profile for the first data points where secondary processes are less significant. After that the wall loss parameters are varied to match the whole time profile. However, for this procedure it is mandatory to know the reasonable range of k_{wall} for each species in the experimental set-up.

The time intervals used for the simulations were typically $\Delta t < 0.1$ s. The yields errors associated with the model were found to be in the range of 0.02. If it is not possible to reproduce the time profiles with the model this will indicate either an error in the spectra evaluation, the simplified mechanism used or the experiments conducted.

3 Results and discussion

All experiments were conducted at a total pressure of 990 ± 15 mbar and 298 ± 3 K. Irreversible first-order wall losses of 3M3P2 and 4M3P2 were found to be negligible in the

480 L chamber and in the range $(1\text{--}6) \times 10^{-5} \text{ s}^{-1}$ and $(1\text{--}8) \times 10^{-5} \text{ s}^{-1}$ in the 1080 L chamber, respectively. In separate control experiments, containing the target species in the bath gas only, no difference was observed for the wall loss in the dark and when the mixture was irradiated over the typical length of an experiment. Hence, an increased wall loss rate due to convection induced by heated walls could be ruled out. Dark reactions between the radical source and the target species were tested as well in separate experiments and were found to be negligible in both reaction chambers. Photolysis of the unsaturated ketones was likewise found to be negligible under the experimental conditions.

3.1 Kinetic study

Relative-rate plots according to Eq. (1) are presented in Fig. 1 for all kinetic experiments conducted. Three reference compounds have been used to determine the rate coefficient of each investigated reaction system. The relative-rate plots for individual experiments display a high linearity, with correlation coefficients from linear regression analysis being $R^2 > 0.95$ and zero intercepts within a 2σ statistical error. The calculated relative ratios $k_{\text{carbonyl}}/k_{\text{ref}}$ are summarized in Table 2. They were found to be independent of the initial concentration of the unsaturated ketone and the irradiation time. In the case of the Cl reactions, the relative ratios were independent of using either synthetic air or nitrogen as bath gas. Therefore, the obtained relative ratios likely result solely from each target reaction and any interfering process can be neglected in the present experimental set-up.

The rate coefficients were calculated based on the determined relative ratios using the following reference data: $k(\text{isobutene} + \text{OH}) = (5.1 \pm 1.0) \times 10^{-11} \text{ cm}^3 \text{ molecule}^{-1} \text{ s}^{-1}$ (Mellouki et al., 2021), $k(\text{propene} + \text{OH}) = (2.9 \pm 0.8) \times 10^{-11} \text{ cm}^3 \text{ molecule}^{-1} \text{ s}^{-1}$ (Atkinson et al., 2006), $k(1,3\text{-butadiene} + \text{OH}) = (6.66 \pm 1.33) \times 10^{-11} \text{ cm}^3 \text{ molecule}^{-1} \text{ s}^{-1}$ (Calvert et al., 2000), $k(\text{isoprene} + \text{OH}) = (1.0 \pm 0.2) \times 10^{-10} \text{ cm}^3 \text{ molecule}^{-1} \text{ s}^{-1}$ (Mellouki et al., 2021), $k(\text{isobutene} + \text{Cl}) = (3.40 \pm 0.28) \times 10^{-10} \text{ cm}^3 \text{ molecule}^{-1} \text{ s}^{-1}$ (Ezell et al., 2002), $k(\text{propene} + \text{Cl}) = (2.64 \pm 0.21) \times 10^{-10} \text{ cm}^3 \text{ molecule}^{-1} \text{ s}^{-1}$ (Ezell et al., 2002), $k(\text{methyl valerate} + \text{Cl}) = (1.7 \pm 0.2) \times 10^{-10} \text{ cm}^3 \text{ molecule}^{-1} \text{ s}^{-1}$ (Notario et al., 1998).

In Table 2 the calculated rate coefficients are given as an average for each reference together with the corresponding error as a combination of the relative ratio's statistical error and the error of the reference's rate coefficient. The determinations with different reference compounds agree within $< 4\%$ for the Cl reactions and $< 17\%$ for the OH reactions, respectively. The final rate coefficients for the target reactions are given as the weighted average of all experimental determinations: $k(3\text{M3P2} + \text{OH}) = (6.5 \pm 1.2) \times 10^{-11} \text{ cm}^3 \text{ molecule}^{-1} \text{ s}^{-1}$, $k(4\text{M3P2} + \text{OH}) = (8.1 \pm 1.3) \times 10^{-11} \text{ cm}^3 \text{ molecule}^{-1} \text{ s}^{-1}$, $k(3\text{M3P2} + \text{Cl}) =$

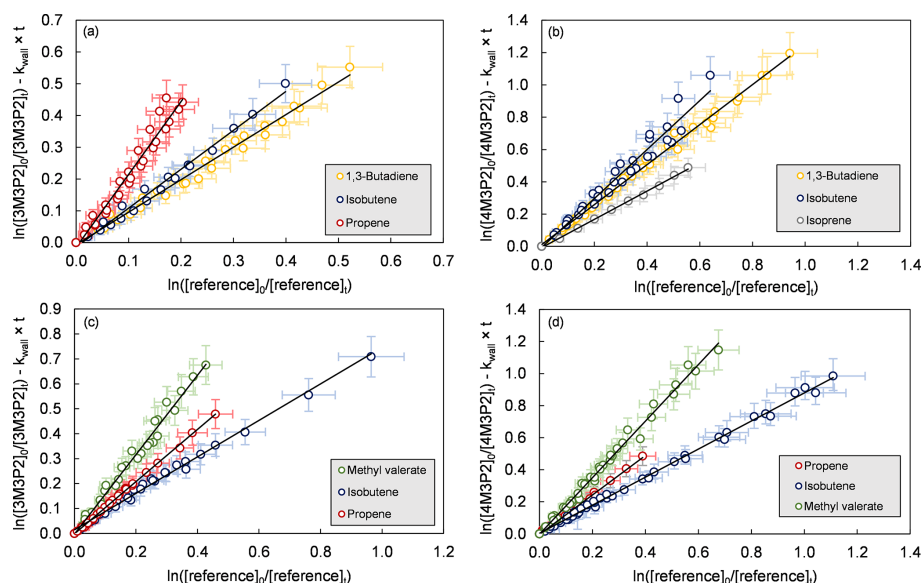


Figure 1. Relative-rate plots of all experiments according to Eq. (1) for the reaction of (a) 3-methyl-3-penten-2-one + OH, (b) 4-methyl-3-penten-2-one + OH, (c) 3-methyl-3-penten-2-one + Cl and (d) 4-methyl-3-penten-2-one + Cl. The error bars consist of a systematic uncertainty and an additional 10 % relative error to cover uncertainties derived from the experimental and evaluation procedure, respectively.

Table 2. Results of the kinetic study using different reference compounds.

Reaction	Reference	Number of runs	Ketone [ppm] ₀	Ketone max. consumption	$k_{\text{carbonyl}}/k_{\text{ref}}$	$k \times 10^{11} / \text{cm}^3 \text{ molecule}^{-1} \text{ s}^{-1}$
4M3P2 + OH	Isobutene	4	5.0–6.0	47 %–65 %	1.47 ± 0.31	7.5 ± 1.8
	1,3-Butadiene	6	0.9–6.0	28 %–70 %	1.29 ± 0.03	8.6 ± 1.9
	Isoprene	1	0.9	39 %	0.88 ± 0.03	8.8 ± 1.3
	Average					8.1 ± 1.3
4M3P2 + Cl	Isobutene	5	0.9–6.0	18 %–63 %	0.90 ± 0.07	30 ± 3
	Propene	3	0.9–6.0	12 %–38 %	1.18 ± 0.09	31 ± 4
	Methyl valerate	4	5.0–6.0	39 %–68 %	1.79 ± 0.12	31 ± 4
	Average					31 ± 4
3M3P2 + OH	Propene	3	0.7–6.1	34 %–37 %	2.37 ± 0.40	6.9 ± 2.1
	Isobutene	2	0.7–6.1	21 %–39 %	1.20 ± 0.02	6.1 ± 0.6
	1,3-Butadiene	3	0.9–6.1	29 %–42 %	1.01 ± 0.06	6.7 ± 1.4
	Average					6.5 ± 1.2
3M3P2 + Cl	Isobutene	4	0.7–6.1	20 %–51 %	0.80 ± 0.14	27 ± 5
	Propene	3	0.7–6.1	17 %–38 %	1.07 ± 0.04	28 ± 3
	Methyl valerate	3	5.0–6.1	37 %–49 %	1.60 ± 0.08	27 ± 3
	Average					28 ± 4

$(2.8 \pm 0.4) \times 10^{-10} \text{ cm}^3 \text{ molecule}^{-1} \text{ s}^{-1}$ and $k(4\text{M3P2}+\text{Cl}) = (3.1 \pm 0.4) \times 10^{-10} \text{ cm}^3 \text{ molecule}^{-1} \text{ s}^{-1}$. The quoted errors represent the 2σ statistical error of the weighted mean and an additional 10 % relative error to cover all uncertainties derived from the experimental and evaluation procedure.

Rate coefficients for the reaction of 4M3P2 with OH radicals and Cl atoms have been previously determined by Gaona-Colmán et al. (2017), using the relative-rate

technique and GC-FID as the detection method. The present values are about 20 % smaller (OH reaction) and 15 % larger (Cl reaction) than those reported by Gaona-Colmán et al. (2017). However, both values are found within the uncertainties of the former study and thus are in good agreement. Wang et al. (2015) reported $k(3\text{M3P2}+\text{Cl}) = (3.00 \pm 0.34) \times 10^{-10} \text{ cm}^3 \text{ molecule}^{-1} \text{ s}^{-1}$ at $293 \pm 1 \text{ K}$ based on a relative-rate study (GC-FID detection) employing large initial mix-

ing ratios for the target species (100 ppm). Nevertheless, the value determined within this work is in excellent agreement with the one reported by Wang and co-workers.

3.1.1 Reactivity

It is generally accepted that OH radical and Cl atom reactions of OVOCs proceed via H atom abstraction or addition to the C=C double bond, in the case of unsaturated organic species. The AOPWIN software (US EPA, 2021; Kwok and Atkinson, 1995) estimates for the OH reaction with both investigated ketones, without discriminating, the contribution of H atom abstraction and OH addition to the olefinic bond to be $k_{\text{abs.}} = 0.4 \times 10^{-12} \text{ cm}^3 \text{ molecule}^{-1} \text{ s}^{-1}$ and $k_{\text{add.}} = 7.8 \times 10^{-11} \text{ cm}^3 \text{ molecule}^{-1} \text{ s}^{-1}$, respectively. This suggests that the OH reaction proceeds almost exclusively through the addition to the C=C double bond. This theoretical result is supported by the findings of the present product studies (see Sect. 3.3). The rate coefficients of 4M3P2 + OH predicted by AOPWIN and determined here experimentally agree within 4%. However, AOPWIN does not differentiate between certain substitution patterns. Given that there is a good agreement between the results using different references, our results show 4M3P2 to be about 1.25 times more reactive towards OH radicals than 3M3P2. Therefore, the AOPWIN prediction is less accurate in the case of 3M3P2. Estimations for the rate coefficients of the reactions of both ketones with OH radicals were given as well in an earlier study ($k(3\text{M3P2} + \text{OH}) = 4.2 \times 10^{-11} \text{ cm}^3 \text{ molecule}^{-1} \text{ s}^{-1}$ and $k(4\text{M3P2} + \text{OH}) = 5.3 \times 10^{-11} \text{ cm}^3 \text{ molecule}^{-1} \text{ s}^{-1}$) based on linear free-energy relationships using ionization potentials (Grosjean and Williams, 1992). Being lower for both ketones, these predictions qualitatively reproduce, however, the experimentally observed rate coefficient ratio $k(4\text{M3P2} + \text{OH})/k(3\text{M3P2} + \text{OH}) \approx 1.26$. The same applies when the estimation of the rate constants is performed according to the SAR approach by Jenkin et al. (2018).

On the other hand, if the reaction proceeds almost solely via the electrophilic addition to the C=C double bond the reactivity can be examined in terms of the electron density associated with the olefinic bond. We have recently pointed out the importance of defining the appropriate core structure when discussing gas-phase reactivity and related substituent effects in unsaturated oxygenated compounds (Illmann et al., 2021a). In the case of the α,β -unsaturated ketones this yields a comparison with structural analogue alkenes where the acetyl moiety is replaced by an H atom, thus (*Z*)-2-butene (for 3M3P2) and isobutene (for 4M3P2) as structural analogues. Despite the deactivating ($-I$) effect of carbonyl groups, the ability of the carbonyl group to form hydrogen-bonded intermediates with OH radicals (Smith and Ravishankara, 2002) lead to a presumably higher reactivity of the unsaturated ketones compared to their alkene analogues. Experimental results supporting this assumption were reported

previously, although the corresponding alkenes were chosen in a different way (Blanco et al., 2012).

An attempt to quantify the substituent effects in oxygenated compounds was previously performed by defining a non-dimensional reactivity factor $x_r = k_{\text{ketone}}/k_{\text{alkene}}$ (Illmann et al., 2021a). By using the latest IUPAC recommendations (Mellouki et al., 2021) for the OH radical reactions of isobutene and (*Z*)-2-butene, respectively, and the results of the present study we obtained for both ketones $x_r > 1$. This is in complete agreement with the expected enhancement of reactivity towards OH radicals. On the other hand, x_r is < 1 for both ketones in the case of the Cl atom reaction. This is not surprising as here the formation of an activating hydrogen-bonded intermediate is not possible. Therefore, the reactivity towards Cl atoms is determined by the deactivating inductive effect of the carbonyl moiety upon the olefinic bond. However, an in-depth analysis of these effects is more related to fundamentals of physical chemistry and will be included in a separate publication.

3.2 Infrared cross sections

Integrated absorption cross sections σ have been determined based on the Beer–Lambert law,

$$\int_{\nu_1}^{\nu_2} \ln\left(\frac{I_0}{I}\right) d\nu = \sigma \times c \times l, \quad (2)$$

by plotting the integrated absorption band between ν_1 and ν_2 against the concentration c . These values are summarized in Table 3 together with literature data where available. Plots used to determine the cross sections are shown in Figs. S1 and S2 in the Supplement. To the best of our knowledge, there are no previous reports on the IR cross sections for 3M3P2, 4M3P2 and acetoin in the literature. Profeta and co-workers (2011) reported band intensities for the various absorptions of biacetyl in the gas phase. The integrated cross section of the carbonyl absorption ($1690\text{--}1769 \text{ cm}^{-1}$) determined within this work is almost identical with their value. The other cross sections agree within $< 10\%$, where the largest discrepancies are observed for the least intense absorption features (between $870\text{--}994$ and $2905\text{--}3053 \text{ cm}^{-1}$).

We recommend using freshly prepared or purchased samples when working with biacetyl. The investigation of an older sample stored for several months at temperatures $< 8^\circ\text{C}$ yielded cross sections 30%–40% lower than those reported by Profeta et al. (2011) while the gas-phase IR spectra were identical with the new sample. Thus, it seems likely that degradation takes place even in a cooled sample. However, the absence of foreign absorption features in the FTIR spectra of the older sample remains unexplained.

In order to determine its integrated absorption cross section, 2-hydroxy-2-methylpropanal (HMPr) was generated in situ through the ozonolysis of 2-methyl-3-buten-2-ol in the presence of sufficient amounts of CO to scavenge any OH radical formed during the reaction. According to the

Table 3. Integrated absorption cross sections determined within this work (resolution: 1 cm^{-1} , apodization: Happ-Genzel, phase correction: Merck, zero-filling: 0) together with available literature references.

Compound	Range/ cm^{-1}	This work	Literature	Reference
		$\sigma \times 10^{18}/\text{cm molecule}^{-1}$	$\sigma \times 10^{18}/\text{cm molecule}^{-1}$	
3-Methyl-3-penten-2-one	1600–1750	35 ± 4		
4-Methyl-3-penten-2-one	1675–1741	17 ± 2		
Acetoin	3100–2700	17 ± 2		
	1766–1704	14 ± 2		
Biacetyl	2905–3053	2.7 ± 0.2	2.9	Profeta et al. (2011)
	1690–1769	31 ± 2	31	Profeta et al. (2011)
	1392–1476	5.1 ± 0.4	5.5	Profeta et al. (2011)
	1297–1392	9.3 ± 0.7	10	Profeta et al. (2011)
	1078–1154	12 ± 1	13	Profeta et al. (2011)
	870–994	3.8 ± 0.4	4.2	Profeta et al. (2011)
2-Hydroxy-2-methylpropanal	2780–3010	30 ± 5	10.2 ± 1.6	Carrasco et al. (2006)

well-established gas-phase ozonolysis mechanism, the initially formed trioxolane will decompose in two possible ways to form either one or the other primary carbonyl, namely formaldehyde (HCHO) and HMP_r, and the remaining Criegee intermediate. A secondary formation of both carbonyls resulting from further reactions of the Criegee intermediates is not likely based on the known mechanism. Moreover, by comparison with FTIR spectra of commercially available epoxides, we do not find any hint for epoxide formation in the gas-phase ozonolysis of 2-methyl-3-buten-2-ol, which is in agreement with previous studies (Carrasco et al., 2007, and references therein). Therefore, the sum of the molar yields of HCHO and HMP_r should yield 100%. The concentrations of HMP_r in each spectrum are thus obtained based on the consumption of the HMP_r-precursor 2-methyl-3-buten-2-ol and the molar formation yield of HMP_r (Y_{HMP_r}),

$$Y_{\text{HMP}_r} = 1 - Y_{\text{HCHO}}, \quad (3)$$

where Y_{HCHO} is the experimentally determined molar formation yield of HCHO. However, in doing so the determined cross section is $(30 \pm 5) \times 10^{-18} \text{ cm molecule}^{-1}$, which is about 300% larger than the only available literature reference (Carrasco et al., 2006). If the literature reference is taken as the true value this would either indicate a fundamental underestimation of the HMP_r concentration or an erroneous determination of the 2-methyl-3-buten-2-ol concentration in our experiments. The unsaturated alcohol is highly volatile and does not pose quantification problems. Moreover, no wall loss was measured in any of the chambers either for the alcohol or for the HMP_r (see Sect. 3.3). A falsely determined cross section of the HMP_r precursor by a factor up to 3 is therefore very unlikely. On the other hand, using the literature cross section would result in molar yields of about 190% for HMP_r in our experiments.

Carrasco et al. (2006) synthesized and purified HMP_r in the liquid phase and evaporated different amounts of the sample. The concentrations were calculated according to the ideal gas law and subtracting the amounts of formic acid and formaldehyde still present in the liquid sample despite purification. Although the authors stated that HMP_r has also been synthesized in situ, similarly to the present study, the cross section seems to be calculated based solely on the liquid sample evaporation. However, the listed integrated cross section for HCHO, based on the natural logarithm as stated by the authors, differs about a factor of 2 from other literature references (Nakanaga et al., 1982; Gratien et al., 2007). As well as this, the used value is about 2.3 smaller than the cited literature reference (Picquet-Varrault et al., 2002). All this suggests a systematic conversion error in the previous study. Therefore, we prefer to use the HMP_r cross section estimated in our group for the following product study.

3.3 Product study of the OH reactions

In the following subsections the terms “ α and β position” are used with respect to their position related to the carbonyl group. Thus, the C_α refers to the carbon atom adjacent to the carbonyl group. Consequently, the $\alpha\text{-RO}_2$ radical names the RO_2 where the molecular oxygen added in α position.

3.3.1 3-Methyl-3-penten-2-one + OH

Figure 2 shows details obtained by evaluating IR spectra recorded during a 3M3P2 + OH experiment and the references used to identify the reaction products. The range $3600\text{--}2600 \text{ cm}^{-1}$ was chosen solely for clarity reasons. More spectra focussing on other spectral ranges can be found in Fig. S3 in the Supplement. Figure S4 in the Supplement shows reference spectra for the unsaturated ketones. The remaining

absorption features present in the residual spectra after subtraction of 3M3P2, methyl nitrite, methyl nitrate, HNO_3 , HONO, HCHO, NO and NO_2 can be unambiguously attributed to acetoin, biacetyl, acetaldehyde and peroxyacetyl nitrate (PAN), respectively. CO_2 formation was clearly observed by examination of its absorption features in the range 2400–2250 cm^{-1} during the irradiation period. After subtraction of all clearly assigned spectral features the residual spectrum contains only weak absorption bands centred on 1654, 1364, 1297 and 856 cm^{-1} . Although a possible indication for the formation of organic nitrates, they are too weak to be reasonably interpreted.

The formation of the identified species can be well explained as first-generation products of the OH-initiated oxidation of 3M3P2, according to the proposed mechanism depicted in Fig. 3. The OH radical is expected to add predominantly to the C=C double bond in either α or β position followed by the addition of O_2 to form the corresponding α - or β - RO_2 radical (= hydroxyperoxy radical). Their formation and further oxidation pathways (Fig. 3) are consecutively defined as α_n and β_n pathways, respectively. Due to the presence of NO in excess, under these experimental conditions it is certain that virtually all RO_2 radicals will react with NO to mainly form the corresponding RO radicals (= hydroxyalkoxy radicals). The β -RO radical can undergo a bond scission (pathway β_1 , Fig. 3) between the α and β carbon (C_α and C_β) to form acetaldehyde and a hydroxyalkyl radical. This, in turn, reacts with O_2 to produce biacetyl. In principle, the H atom abstraction from the β -RO by O_2 might lead to the formation of a 2-hydroxy-1,3-dicarbonyl species (pathway β_2 , Fig. 3). However, after subtraction of all identified species there are no remaining IR absorption bands to support the occurrence of this pathway. On the other hand, the reaction of RO_2 with NO is known to be exothermic, resulting in chemically activated RO radicals potentially prone to “prompt” decomposition (Orlando et al., 2003). This pathway was shown to be important for RO radicals where energy barriers to decomposition are low, as expected for the β -RO radical according to available estimation methods (Atkinson, 2007; Vereecken and Peeters, 2009). As well as this, Atkinson (2007) concluded that decomposition will dominate compared to the reaction with O_2 in the case of 1,2-hydroxyalkoxy radicals. This also applies for the thermalized hydroxyalkoxy radicals. All this suggests that either pathway β_2 does not exist if the precursor β -RO radical is formed through $\text{RO}_2 + \text{NO}$ or its branching fraction is very low.

The addition of the OH radical in β position followed by the addition of O_2 and reaction with NO yields eventually acetoin (pathways α and α_1 , Fig. 3). The bond scission in the α -RO radical between C_α and the carbon atom of the carbonyl moiety (pathway α_1 , Fig. 3) yields further acetyl radicals which, after addition of O_2 , can either form peroxyacetyl nitrate (through addition of NO_2) or react with NO to finally form CO_2 and HCHO, under the experimental conditions.

The yield of HCHO related to 3M3P2 oxidation cannot be experimentally determined because it is also produced in the methyl nitrite photolysis itself. On the other hand, the α -RO radical can also form biacetyl if the bond scission occurs between C_α and C_β (pathway α_2 , Fig. 3). In this case acetaldehyde evolves from the simultaneously formed hydroxyalkyl radical due to H atom abstraction through molecular oxygen.

3.3.2 4-Methyl-3-penten-2-one + OH

Figure 4 depicts evaluation details of IR spectra recorded during a product study experiment of 4M3P2 and references. The spectral range 3200–2600 cm^{-1} was chosen as mentioned above. Acetone, methyl glyoxal and peroxyacetyl nitrate are clearly identifiable in all residual spectra after subtraction of 4M3P2, methyl nitrite, methyl nitrate, HNO_3 , HONO, HCHO, NO and NO_2 . As in the 3M3P2 product studies, the CO_2 formation during the irradiation period was unambiguously observed in the range 2400–2250 cm^{-1} (Fig. S5 in the Supplement). Trace (f) in Fig. 4 shows an exemplary residual spectrum after subtraction of methyl glyoxal, acetone and PAN references from the spectrum in trace (c). The spectral features are in excellent agreement, in the presented range, with a reference IR spectrum of 2-hydroxy-2-methylpropanal (see Sect. 3.2). This proves its formation in the OH-radical-initiated oxidation of 4M3P2. After subtraction of all assigned absorptions the remaining residual spectra, in both 480 and 1080 L product study experiments, contain weak but well-defined absorption bands centred around 3478, 1722, 1654, 1297 and 856 cm^{-1} (Fig. 5). The characteristic absorption pattern of the latter three bands is a strong indication for organic nitrate formation in this reaction system.

Based on the experimental results obtained here a mechanism for the reaction of OH radicals with 4M3P2 was drawn (Fig. 6). The OH radical will add predominantly to either the α or β carbon. The subsequent O_2 addition will yield the corresponding β - or α - RO_2 radical, respectively. As for 3M3P2, all 4M3P2 product studies were conducted under conditions where RO_2 radicals are expected to react solely with NO. Acetone can be formed from the conversion of the β - RO_2 with NO into the corresponding β -RO followed by the scission of the C–C bond between C_α and C_β (pathway β_1 , Fig. 6). The synchronously generated hydroxyalkyl radical might react with O_2 to yield methyl glyoxal. HMPn formation can be explained by a bond scission between C_α and the carbon atom of the carbonyl group (pathway α_1 , Fig. 6). In the present experimental system, the co-generated acetyl radicals yield either PAN or CO_2 and HCHO, as discussed above. Methyl glyoxal and acetone can also be formed according to pathway α_2 (Fig. 6) if the bond scission in the α -RO occurs between C_α and C_β .

Hypothetically, the α -RO radical could also produce a 3-hydroxy-1,2-dicarbonyl species (pathway α_3 , Fig. 6) if H atom abstraction via molecular oxygen would occur rather

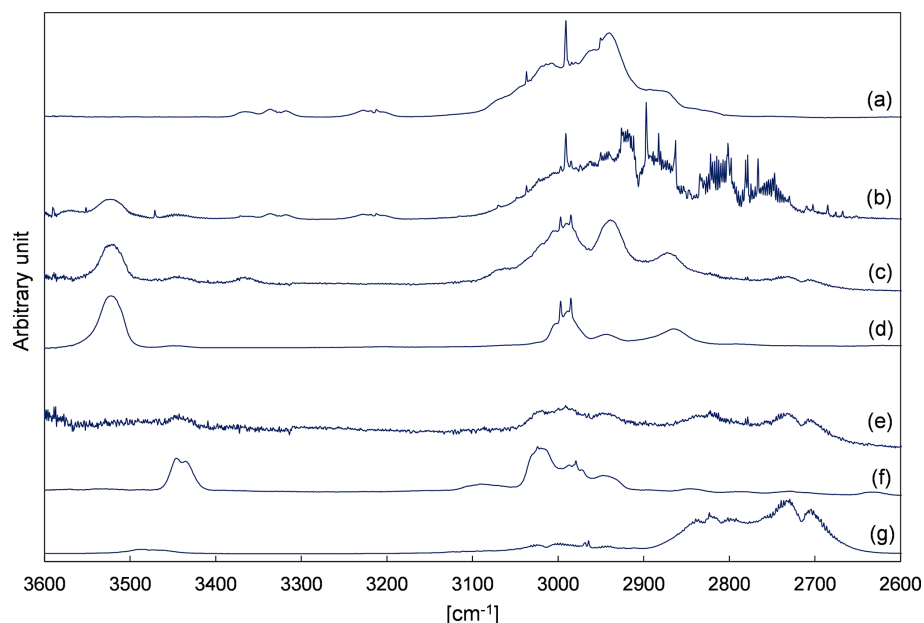


Figure 2. Exemplary FTIR spectra of a product study experiment of 3M3P2 + OH: (a) reaction mixture before irradiation; (b) reaction mixture at the end of the irradiation period; (c) residual spectrum after subtraction of methyl nitrite, methyl nitrate, HNO₃, HONO, NO, NO₂ and HCHO from (b); (d) reference spectrum of 3-hydroxy-2-butanone (acetoin); (e) residual spectrum after subtraction of 3M3P2 and acetoin from (c); (f) reference spectrum of 2,3-butanedione (biacetyl); and (g) reference spectrum of acetaldehyde. The spectra are shifted and scaled individually for a better overview.

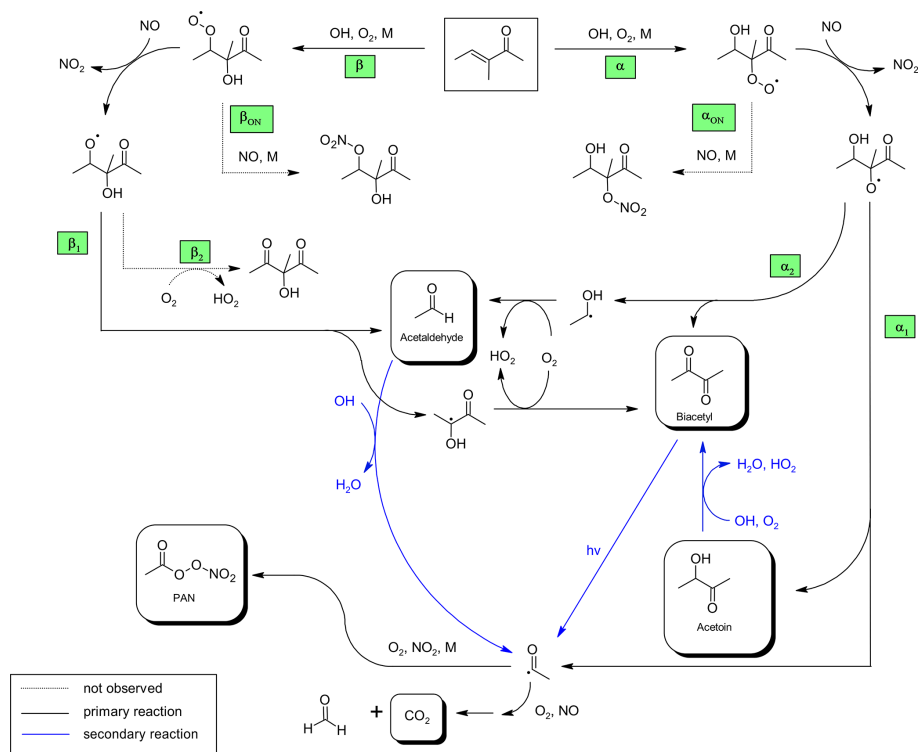


Figure 3. Proposed mechanism for the OH-radical-initiated oxidation of 3-methyl-3-penten-2-one and further oxidation of the first-generation products relevant under the experimental conditions.

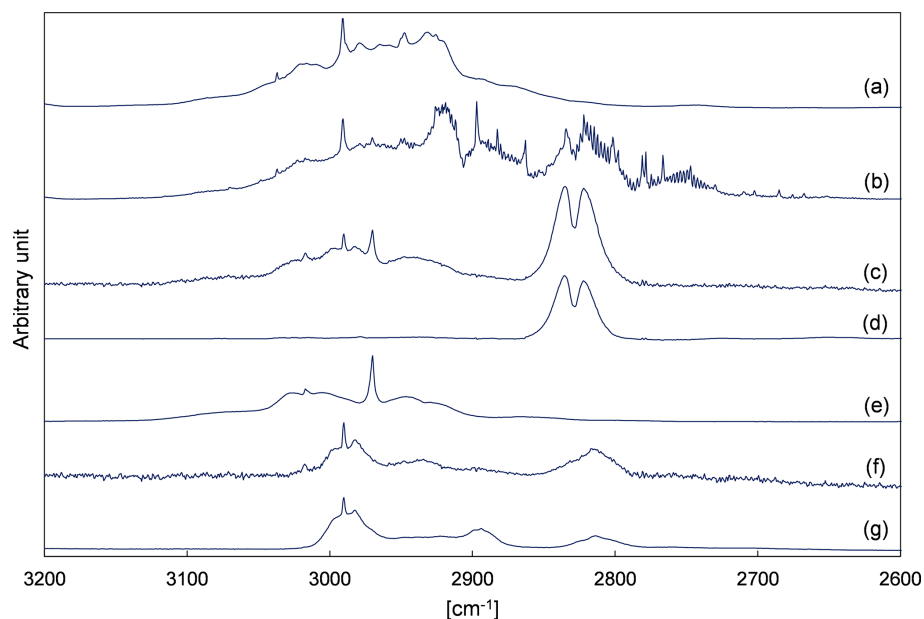


Figure 4. Exemplary FTIR spectra of a product study experiment of 4M3P2 + OH: (a) reaction mixture before irradiation; (b) reaction mixture at the end of the irradiation period; (c) residual spectrum after subtraction of 4M3P2, methyl nitrite, methyl nitrate, HONO, HNO₃, NO, NO₂ and HCHO from (b); (d) reference spectrum of methyl glyoxal; (e) reference spectrum of acetone; (f) residual spectrum after subtracting methyl glyoxal, acetone and PAN from (c); and (g) reference spectrum of 2-hydroxy-2-methylpropanal generated in situ. The spectra are shifted and scaled individually for a better overview.

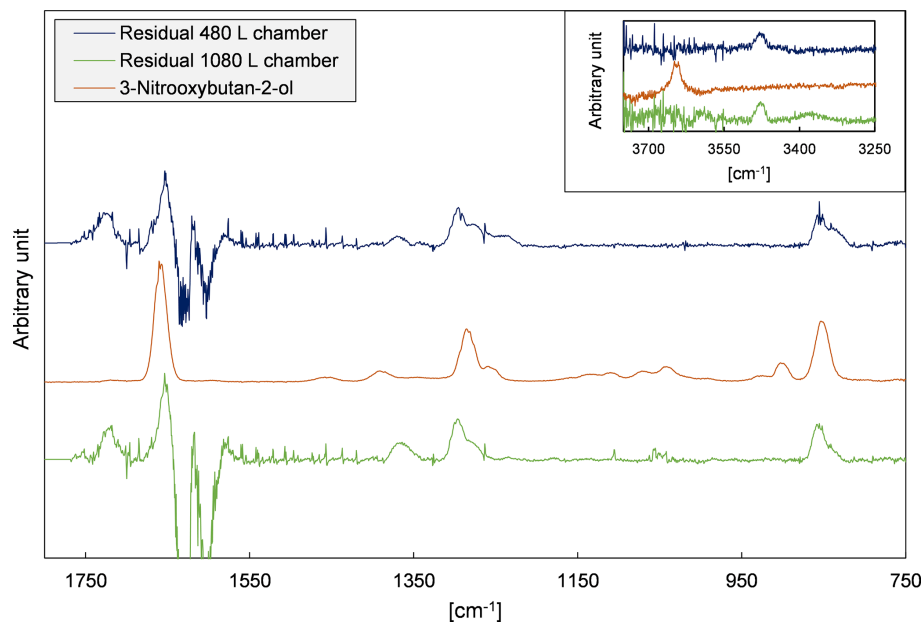


Figure 5. Residual spectra of 4M3P2 + OH product study experiments performed in both chambers after subtraction of all identified species and an exemplary reference spectrum of an organic nitrate recorded in our laboratory (Spittler, 2001).

than a C–C bond scission. However, the structure of the weak carbonyl absorption in the residual spectra seems more likely to belong to a single C=O bond rather than a vicinal diketone. There is thus no indication for the existence of this reaction pathway. Besides, the reaction $\text{RO} + \text{O}_2$ is not ex-

pected to be competitive to the decomposition channels of the multifunctional RO radical, as discussed above.

Organic nitrate formation, which is indicated by the residual spectra, is expected to proceed through the reaction of the $\alpha\text{-RO}_2$ or $\beta\text{-RO}_2$ radical with NO (pathway α_{ON} or β_{ON} ,

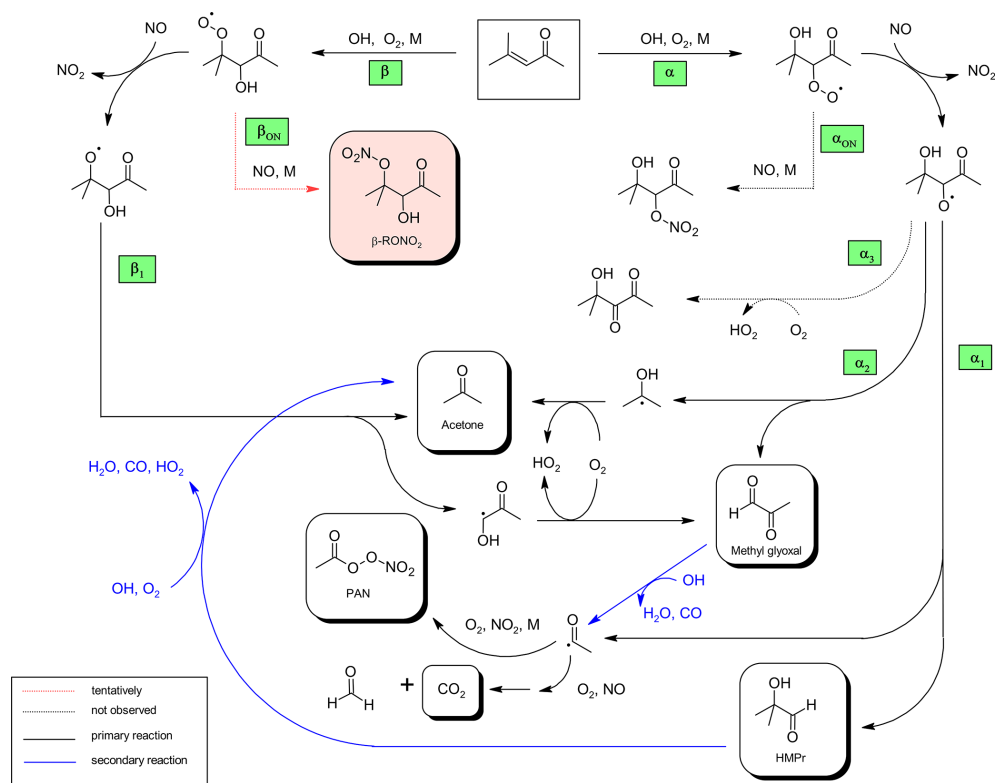


Figure 6. Proposed mechanism for the OH-radical-initiated oxidation of 4-methyl-3-penten-2-one and further oxidation of the first-generation products relevant under the experimental conditions.

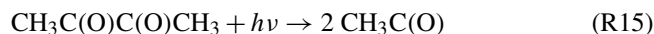
Fig. 6) followed by the isomerization of the nascent ROONO adduct (Calvert et al., 2015). RONO₂ formation has also been observed through RO + NO₂ reactions of simple alkoxy radicals (Frost and Smith, 1990; Mund et al., 1998). However, high-pressure rate coefficients for these types of reactions are about $(1-3) \times 10^{-11} \text{ cm}^3 \text{ molecule}^{-1} \text{ s}^{-1}$ (Atkinson et al., 2006), whereas for the reactions of RO with O₂, $k \times [\text{O}_2]$ is about $4 \times 10^4 \text{ s}^{-1}$ according to a recommendation provided by Atkinson (2007). Given that RO + O₂ seems even not to compete with unimolecular decomposition for β -hydroxyalkoxy radicals we do not expect RO + NO₂ to be experimentally and atmospherically relevant. The absorption features observed in the residual spectra, additionally to the characteristic nitrate absorptions, indicate the presence of a carbonyl (1722 cm^{-1}) and an OH group (3478 cm^{-1}) which can be assigned to multifunctional hydroxycarbonyl nitrates as presented in Fig. 6. In the case of the RONO₂ species resulting from the α -RO radical, one would expect that intramolecular hydrogen bonding between the OH- and the carbonyl group stabilize the structure. This would cause, on the one hand, a broader and weaker OH absorption band and, on the other hand, a shift of the carbonyl absorption towards lower wavenumbers. Based on that, it is more likely that the residual absorptions to the hydroxycarbonyl nitrate result from the β -RO₂ radical. The formation of organic nitrates will be further discussed in Sect. 3.3.5.

3.3.3 Product yields correction and further oxidation processes

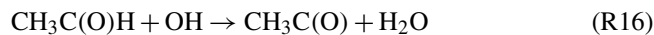
Product yields were obtained by plotting their mixing ratio versus the mixing ratio of consumed unsaturated ketone. The data are corrected only for the wall loss of the unsaturated ketones. These plots are shown in Figs. S6 and S7 in the Supplement and exhibit a high linearity for all identified products except for PAN, CO₂, or the sum of PAN and CO₂. The latter was used to determine the molar formation yield of acetyl radicals. The non-linearity is a strong indication for further oxidation and secondary processes in the investigated reaction systems leading to acetyl radicals and their further oxidation products. However, this can be well explained by the oxidation of the initially formed reaction products in the OH-radical-initiated oxidation of the unsaturated ketones. On the other hand, the linearity, observed for the other oxidation products, does not necessarily indicate the absence of secondary processes. Either secondary formation compensates for loss processes or the scattering of the combined data is larger than the precise non-linearity.

According to Aschmann et al. (2000) the OH-initiated oxidation of acetoin proceeds predominantly through alkyl H atom abstraction at the $-\text{CH}(\text{OH})$ entity to eventually yield biacetyl, with a formation yield of about 80%. This is also expected to be the main loss process under atmospheric con-

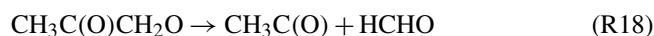
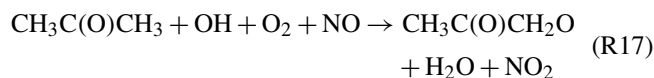
ditions. Therefore, the further oxidation of acetoin is an additional source of biacetyl in the 3M3P2 experimental system. Biacetyl itself is mainly subject to photolysis (R15), under both the present experimental and atmospheric conditions yielding acetyl radicals.



Acetaldehyde also contributes to the formation of acetyl radicals since the aldehydic H atom abstraction (Reaction R16) was shown to account for about 95 % of the OH reaction (Calvert et al., 2011).



Acetone, formed in the oxidation of 4M3P2, will be mainly oxidized by OH radicals through H atom abstraction yielding acetonoxyl radicals which readily decompose to HCHO and acetyl radicals (Orlando et al., 2000).



However, while being a source of HCHO and acetyl radicals under atmospheric conditions, this reaction cannot play any role in the present experimental set-up, considering the lifetime of acetone with respect to OH. By contrast, HMP_r was shown to display a much higher reactivity towards OH, the reaction producing acetone with a yield of unity (Carrasco et al., 2006). Thus, this is a secondary source of acetone in our experiments. Finally, the OH reaction of methyl glyoxal will exclusively proceed via the abstraction of the aldehydic H atom. The initially formed $\text{CH}_3\text{C}(\text{O})\text{CO}$ radical will readily dissociate into carbon monoxide and $\text{CH}_3\text{C}(\text{O})$ radicals as well (Green et al., 1990). Based on the lamp spectrum we calculated the photolysis frequency of methyl glyoxal for all experimental conditions. The ratio between $k(\text{CH}_3\text{C}(\text{O})\text{CHO} + \text{OH}) \times [\text{OH}]$ and $J(\text{CH}_3\text{C}(\text{O})\text{CHO})$ was found to be typically > 7 . Hence, while photolysis of methyl glyoxal is the main loss process under most atmospheric daytime conditions the OH reaction dominates in the present experimental system.

All these processes interfere in the determination of the intrinsic yield of $\text{CH}_3\text{C}(\text{O})$ radicals in the reaction of the unsaturated ketones with OH. As discussed above, the further chemistry of acetyl radicals in our experiments may evolve either into PAN or CO_2/HCHO formation. However, in the atmosphere the readily formed acetyl peroxy radical may also react with HO_2 radicals to form peroxyacetic acid ($\text{CH}_3\text{C}(\text{O})\text{OOH}$), acetic acid ($\text{CH}_3\text{C}(\text{O})\text{OH}$), O_3 and OH radicals (Winiberg et al., 2016). Therefore, in order to evaluate the atmospheric importance of the studied ketones an estimation of the acetyl radicals yield is needed.

The product yields corrected for the secondary reactions mentioned above and wall losses in the simulation chambers

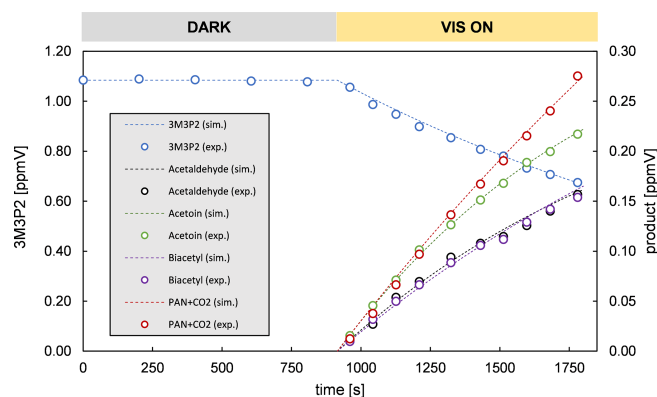


Figure 7. Experimental and simulated time profiles obtained for a 3M3P2 + OH experiment.

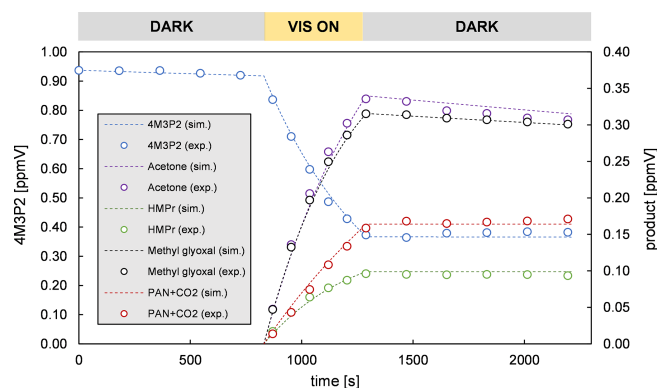


Figure 8. Experimental and simulated time profiles obtained for a 4M3P2 + OH experiment.

were obtained using the model outlined in Sect. 2.7 and the kinetic parameters listed in Tables S1 and S2 in the Supplement. The molar yields for both OH reactions are summarized in Tables 4 and 5. The sum of PAN and CO_2 is equal to the molar yield of $\text{CH}_3\text{C}(\text{O})$ radicals. The errors represent the 2σ statistical error resulting from the average of all experiments and an additional 10 % relative error to cover further uncertainties derived from the evaluation procedure. Exemplary experimental and simulated time profiles of the ketones and the products are shown in Figs. 7 and 8 for both investigated reaction systems.

Acetoin and acetaldehyde are only affected by secondary consumption. Hence, the model estimates an increase for both yields compared to the experimental values of the 3M3P2 oxidation. By contrast, the biacetyl yields exhibit no difference indicating that the loss by photolysis is nearly compensated for by the formation through acetoin oxidation. Both acetaldehyde and biacetyl undergo further oxidation eventually forming PAN and CO_2 . In compliance, the experimental concentration–time profile for acetyl radicals is only reproduced when introducing significantly lower PAN + CO_2 formation yields in the model. In the 4M3P2

Table 4. Uncorrected and corrected molar yields of the 3M3P2 + OH system.

	Acetoin	PAN + CO ₂	Biacetyl	Acetaldehyde
Uncorrected	0.53 ± 0.13	0.69 ± 0.11	0.42 ± 0.13	0.36 ± 0.09
Corrected	0.60 ± 0.18	0.60 ± 0.07	0.41 ± 0.12	0.42 ± 0.15

Table 5. Uncorrected and corrected molar yields of the 4M3P2 + OH system.

	Acetone	Methyl glyoxal	HMPPr	PAN + CO ₂
Uncorrected	0.64 ± 0.11	0.58 ± 0.13	0.17 ± 0.05	0.27 ± 0.04
Corrected	0.62 ± 0.09	0.64 ± 0.16	0.20 ± 0.05	0.24 ± 0.06

system the modelled acetone yield decreases slightly due to the further oxidation of HMPPr. Since methyl glyoxal and HMPPr are influenced only by consumption processes, their corrected yields are higher than those experimentally determined. PAN + CO₂ correction follows the same pattern as in the case of 3M3P2 + OH.

In all cases the averaged molar yields are in excellent agreement for products expected to be formed in the same reaction channel. Thus, the molar yields of acetaldehyde/biacetyl (pathway β_1 and α_2 , Fig. 3), acetoin/(PAN + CO₂) (pathway α_1 , Fig. 3) and acetone/methyl glyoxal (pathway β_1 and α_2 , Fig. 6) are nearly the same. In the case of 4M3P2 + OH, the yields of HMPPr/(PAN + CO₂) formed according to pathway α_1 (Fig. 6) are still in good agreement within the uncertainties. This supports the absorption cross section of HMPPr determined in our study. On the other hand, the results prove that the formation of acetyl radicals can be well quantified by determining the sum of PAN and CO₂ in the experimental set-up.

Among α,β -unsaturated ketones of atmospheric importance only the OH-radical-initiated oxidation of methyl vinyl ketone (MVK) has been investigated in depth (Tuazon and Atkinson, 1989; Galloway et al., 2011; Praske et al., 2015; Fuchs et al., 2018). Tuazon and Atkinson (1989) quantified methyl glyoxal and glycolaldehyde as the main oxidation products and concluded that addition of the OH radical to the internal and terminal carbon atom accounts for 28 ± 9 % and 72 ± 21 %, respectively. This calculation is based on the assumption that the corresponding α -RO radical will favour a bond scission between the carbonyl carbon atom and C _{α} (according to pathway α_1 in Figs. 3 and 6) due to the much lower predicted energy barrier to decomposition following this pathway (Tuazon and Atkinson, 1989). This has been confirmed by calculations performed by Praske et al. (2015) and is consistent with the SAR provided by Vereecken and Peeters (2009). Assuming $\alpha_1 \gg \alpha_2$ (Figs. 3 and 6) the addition of OH according to the α and β pathways consequently accounts for 60 ± 18 % and 40 ± 12 % for 3M3P2 and 26 ± 8 % and 74 ± 22 % in the case of 4M3P2, respectively, when referenced to the corresponding overall yield. However, at least

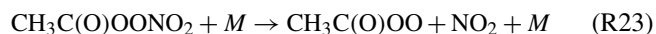
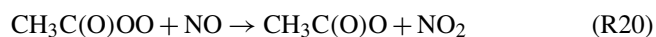
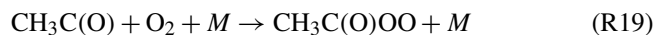
for 4M3P2 the branching fraction α_2 may be important since the estimated energy barrier is lower than for α_1 according to the SAR of Vereecken and Peeters (2009). Hence, one should note that the fraction given for the addition to C _{β} (α pathways) represents a lower limit and an upper limit for the addition of OH to C _{α} (β pathways), respectively. In the limiting case ($\alpha_1 \gg \alpha_2$) this indicates the relationship between the branching ratios of the main channels to be $\alpha > \beta$ for MVK, $\alpha \approx \beta$ for 3M3P2 and $\alpha < \beta$ for 4M3P2 (see Figs. 3 and 6). Due to hyperconjugation the formation of the higher substituted alkyl radical should be favoured. The addition of OH to C _{α} leads to a primary alkyl radical in the case of MVK, a secondary alkyl radical for 3M3P2 and a tertiary alkyl radical in the case of 4M3P2. Therefore, while hydrogen bonding should yield a preference of the addition to the β position for all α,β -unsaturated ketones, as discussed previously with respect to the reactivity, the observed trend in the branching ratios (in the limiting case $\alpha_1 \gg \alpha_2$) is possibly related to the stability of the initially formed alkyl radicals. In the case of 4M3P2 the addition to the β position could also be sterically hindered.

However, one should emphasize that it is not possible to derive the exact branching ratios for α and β without deciphering the branching ratios α_1 and α_2 . An attempt to obtain the corresponding rate coefficients for each decomposition channel according to Vereecken and Peeters (2009) failed since the calculated branching ratios for α_1 and α_2 are about 0.1 and 0.9, respectively, in the case of 4M3P2 which is contradicted by the observed first-generation yields of 2HMPPr and PAN + CO₂. Vereecken and Peeters (2009) stated the accuracy of the predicted rate coefficients to be within a factor of 5–10. Therefore, it is not possible to derive any further statement on the ratio $\alpha_1 : \alpha_2$.

3.3.4 ROONO₂ formation

To further elucidate the mechanism, experiments were conducted over a wider range of NO₂/NO ratios by adding different amounts of NO₂ to the reaction mixture. In all experiments the amount of added NO was sufficient to suppress any ozone formation.

Given that $\text{CH}_3\text{C}(\text{O})$ radicals instantaneously react with oxygen, under the employed experimental conditions, to form the corresponding RO_2 radical, their fate should be described by (a) the reaction with NO , (b) the reaction with NO_2 to yield peroxyacetyl nitrate (PAN), and (c) the thermal dissociation of PAN to re-generate the RO_2 radical.



Based on the Reactions (R20)–(R23) the ratio PAN/CO_2 should only depend on the NO_2/NO ratio during the reaction under constant pressure and temperature conditions. Therefore, PAN/CO_2 ratios were simulated for various NO_2/NO ratios in the experimental temperature range 295–301 K using the IUPAC recommendations (Atkinson et al., 2006) for the Reactions (R20), (R22) and (R23) (Fig. 9). Experimental PAN/CO_2 formation ratios were derived from plotting the generated PAN against the formed CO_2 during the irradiation period. The corresponding average NO_2/NO ratios were determined by averaging the measured mixing ratios of NO and NO_2 , respectively, over the same time interval. As can be seen in Fig. 9, these data are qualitatively in quite good agreement with the expected ratios based on the model calculations. Hence, the fate of the $\text{CH}_3\text{C}(\text{O})$ radicals is well-described by the Reactions sequence (R19)–(R23) in our experiments.

However, in typical methyl nitrite photolysis experiments the NO_2/NO ratios are < 1 if NO is added to suppress ozone formation. Thus, PAN accounts for less than one-third of the $\text{CH}_3\text{C}(\text{O})$ radical's fate (Fig. 9). If the experimental set-up does not allow HCHO or CO_2 to be quantified, this leads to a fundamental underestimation of the acetyl radical reaction channels. In this case, addition of NO_2 could be useful to favour PAN formation and the determination of the NO_2/NO ratio in the experiment could yield an estimation of the PAN/CO_2 ratio.

On the other hand, Fig. 9 clearly shows the invariance of the $\text{PAN} + \text{CO}_2$ yield for 4M3P2 under all experimental conditions, within the uncertainties. There is thus likely no ROONO_2 formation from the initially formed α - and β - RO_2 radicals since they are either not formed or their thermal dissociation is too large to play any role. This meets one's expectations as, according to literature references (Calvert et al., 2015), the lifetimes of alkylperoxy nitrates are of the order of seconds at 298 K and 1 atm and so they become relevant as a NO_x reservoir when formed at lower temperatures, encountered in the upper troposphere. However, assuming an average OH concentration of $1 \times 10^6 \text{ cm}^{-3}$ (Bloss et al., 2005) the atmospheric lifetime (with respect to OH) is about 3.4 h, thus too short for 4M3P2 to enter higher alti-

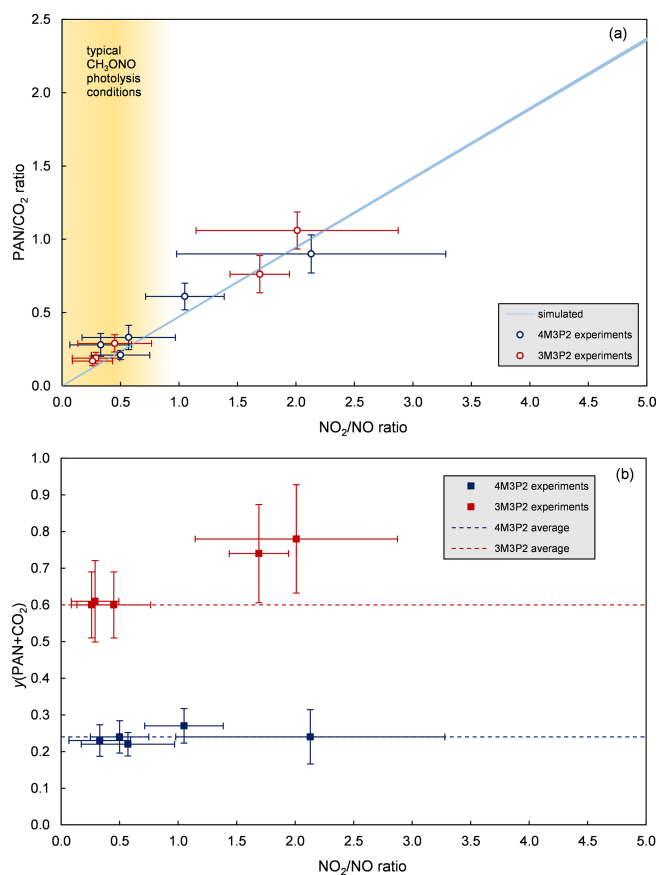


Figure 9. (a) Experimentally determined and simulated PAN/CO_2 formation ratio as a function of the NO_2/NO ratio. (b) Determined molar yields for acetyl radicals (as the sum of PAN and CO_2) as a function of the NO_2/NO ratio.

tudes. Therefore, except for PAN, ROONO_2 formation does not play any role for 4M3P2.

In the case of 3M3P2 significantly higher yields for $\text{PAN} + \text{CO}_2$ were observed for higher NO_2/NO ratios while being quite consistent at $\text{NO}_2/\text{NO} < 1$ (Fig. 9). This is actually contradictory as additional ROONO_2 formation from the initial α - and β - RO_2 radicals should lower the overall yields of the main products. However, the molar yields of biacetyl and acetaldehyde are essentially the same as in the other experiments. Thus, the carbon balance exceeds 100 % in the higher NO_2/NO ratio experiments. Unfortunately, these two experiments were the last in a series and it is quite probable that due to wall loading the wall acted as a source of $\text{CH}_3\text{C}(\text{O})$ radicals during the irradiation. The yield for $\text{PAN} + \text{CO}_2$ was therefore only given as an average of the experiments with $\text{NO}_2/\text{NO} < 1$.

3.3.5 RONO_2 formation

Given that the carbon balance is about one for 3M3P2 and about 0.85 for 4M3P2, respectively, this results in an up-

Table 6. Estimated tropospheric lifetimes for the studied α,β -unsaturated ketones. The lifetimes were calculated using the following concentrations: ^a global mean of 1×10^6 molecules cm^{-3} (Bloss et al., 2005), ^b 12 h average of 3×10^4 molecules cm^{-3} (Wingenter et al., 1996), ^c 24 h average of 7×10^{11} molecules cm^{-3} (Logan, 1985), and ^d 12 h average of 5×10^8 molecules cm^{-3} (Atkinson, 1991). Rate coefficients were taken from: ^e this work, ^f Illmann et al. (2021a), and ^g Canosa-Mas et al. (2005).

Compound	$\tau(\text{OH})^{\text{a}}/\text{h}$	$\tau(\text{Cl})^{\text{b}}/\text{h}$	$\tau(\text{O}_3)^{\text{c}}/\text{h}$	$\tau(\text{NO}_3)^{\text{d}}/\text{h}$
3M3P2	4.3 ^e	33.1 ^e	5.0 ^f	3.6 ^g
4M3P2	3.4 ^e	29.9 ^e	47.2 ^f	3.9 ^g

per limit of the overall RONO_2 yield of 0.15 for 4M3P2 while almost no RONO_2 formation occurs in the case of 3M3P2. This is qualitatively in good agreement with the residual spectra, clearly indicating the presence of organic nitrates only in the case of 4M3P2. Noda et al. (2000) determined an average absorption cross section of $(1.25 \pm 0.20) \times 10^{-17}$ $\text{cm}^2 \text{molecule}^{-1}$ (base 10) for the nitrooxy group absorption in the range 800–900 cm^{-1} by averaging available absorption cross sections of organic nitrates. Following this approach, an estimated RONO_2 yield of 0.06 ± 0.03 is determined, which should be regarded as lower limit. While the determined wall loss is of the order of $2 \times 10^{-4} \text{ s}^{-1}$ the potentially formed RONO_2 species could also be subject of photolysis and oxidation by OH radicals. SAR methods for the prediction of OH rate coefficients were shown to fail at carbonyl nitrates (Suarez-Bertoa et al., 2012). Therefore, Suarez-Bertoa et al. (2012) proposed alternative substituent factors optimized for carbonyl nitrates in which the factor for the $-\text{ONO}_2$ group is less deactivating than in other SAR approaches. Applying this factor to the SAR of Kwok and Atkinson (1995) yields predicted rate coefficients of 1.3×10^{-12} and $5 \times 10^{-13} \text{ cm}^3 \text{ molecule}^{-1} \text{ s}^{-1}$ for the $\alpha\text{-RONO}_2$ and $\beta\text{-RONO}_2$, respectively, which would correspond to loss rates of about 1.3×10^{-5} and $5 \times 10^{-6} \text{ s}^{-1}$, respectively, due to the OH reaction. For α - and β -carbonyl nitrates it was shown that photolysis dominates over the OH-initiated oxidation (Suarez-Bertoa et al., 2012; Picquet-Varrault et al., 2020). Hence, by comparison with available data (Suarez-Bertoa et al., 2012; Picquet-Varrault et al., 2020) larger loss rates likely result from photolysis of the RONO_2 species in our experiments. However, we believe that any further statement would be highly speculative. A RONO_2 yield of about 0.11 ± 0.03 has been reported for MVK based on model-assisted isoprene photooxidation experiments (Paulot et al., 2009). On the other hand, an overall RONO_2 yield of about 0.040 ± 0.006 has been determined in MVK oxidation experiments (Praske et al., 2015). Thus, the limits (0.06–0.15) reported here for the overall organic nitrate yield are consistent with the data dispersion found in the literature.

If the branching fractions for the pathways α_{ON} and β_{ON} in the 4M3P2 oxidation (Fig. 6) were the same this would correspond to a much larger formation yield of the multifunctional $\beta\text{-RONO}_2$ than $\alpha\text{-RONO}_2$ simply due to the predominant addition of the OH radical to C_α . This would be consis-

tent with the previous assignment of the residual's spectral features to the $\beta\text{-RONO}_2$. Former studies on alkenes have shown a structure-dependent RONO_2 yield derived from β -hydroxyperoxy radicals. Accordingly, the nitrate yields resulting from tertiary RO_2 were larger than those produced from secondary RO_2 , which, in turn, were larger when compared to nitrate yields obtained from primary RO_2 (Matsunaga and Ziemann, 2010). This would indicate $\beta_{\text{ON}} > \alpha_{\text{ON}}$ in the 4M3P2 oxidation (Fig. 6). Besides, Praske et al. (2015) found a 2-times-larger branching ratio for the $\beta\text{-RONO}_2$ species resulting from MVK + OH than for the $\alpha\text{-RONO}_2$. They interpreted this finding in terms of a larger destabilizing effect on the initially formed ROONO complex caused by the closer carbonyl group in the case of the $\alpha\text{-RONO}_2$. Both results further support the assignment of the residual absorptions to the $\beta\text{-RONO}_2$ species.

By contrast, both potentially formed RONO_2 species in the 3M3P2 oxidation would contain a quaternary C_α atom surrounded by bulky substituents. Thus, the almost negligible nitrate formation in the case of 3M3P2 is possibly attributed to the steric hindrance of the hypothetically resulting RONO_2 species.

4 Atmospheric implications and conclusions

Within this work we determined the rate coefficients for the OH radical and Cl atom-initiated oxidation of 3M3P2 and 4M3P2. This adds to the kinetic information concerning the reaction of these two compounds with NO_3 and O_3 reported previously (Sato et al., 2004; Canosa-Mas et al., 2005; Illmann et al., 2021a; Li et al., 2021) in an effort to complete the gaps in the knowledge needed for modelling chemistry in the atmosphere. The yields for the identified products formed in both target reactions were found to be independent of the chamber used, the mixing ratios and the light intensity, thus giving confidence in the experimental results.

Using the kinetic data together with reasonable average concentrations for the respective oxidants (Logan, 1985; Atkinson, 1991; Wingenter et al., 1996; Bloss et al., 2005) allows tropospheric lifetimes to be estimated as presented in Table 6, where $\tau(X)$ is the lifetime with respect to the oxidant X calculated according to $1/(k_x[X])$. Both unsaturated ketones did not show measurable photolysis rates in the present experimental set-up. In the atmosphere, their photodissoci-

ation lifetimes are expected to have a range of the order of days (Mellouki et al., 2015). Consequently, compared to $\tau(\text{OH})$, the photodissociation of both unsaturated ketones is evidently not an important process in the troposphere. The values in Table 6 indicate the OH radical as the dominant sink during daytime whereas the NO_3 radical plays a similar role at night. However, for 3M3P2 the O_3 reaction appears quite competitive during both day and night (Table 6). These estimated lifetimes indicate an oxidative degradation near the emission sources. Nevertheless, a further part of this work indicates that both ketones potentially impact atmospheric processes on a larger scale due to their huge potential of forming NO_x reservoir species like PAN. In this respect, we have shown that the reaction of OH with both 3M3P2 and 4M3P2 yields $\text{CH}_3\text{C}(\text{O})$ radicals by prompt decomposition of primary formed RO radicals. In the present work the sum of PAN and CO_2 could be used successfully to determine the formation yield of $\text{CH}_3\text{C}(\text{O})$ radicals in both reaction systems. Moreover, nearly all other identified oxidation products like methyl glyoxal, acetone, acetaldehyde, acetoin and biacetyl are known to generate $\text{CH}_3\text{C}(\text{O})$ radicals in their further oxidation processes – simulations based on field data collected worldwide estimate that acetaldehyde, methyl glyoxal and acetone within the troposphere account for about 81 % of the global source for PAN formation (Fischer et al., 2014). Among the oxidation products of both 3M3P2 and 4M3P2 at least methyl glyoxal is a well-known source of secondary organic aerosol in atmosphere (Fu et al., 2008).

On the other hand, future work is needed to identify clearly the missing products of the OH-radical-initiated oxidation of 4M3P2. The absorptions of the residual spectra could be tentatively assigned to the β -RONO₂ species. However, other detection methods are necessary for an unambiguous identification and quantification of this species.

Data availability. Data can be provided upon request to the corresponding author.

Supplement. The supplement related to this article is available online at: <https://doi.org/10.5194/acp-21-13667-2021-supplement>.

Author contributions. NI, RGG and IPK conducted the experiments and processed the data. NI developed the model and performed the calculations. NI prepared the paper with contributions from all co-authors.

Competing interests. The contact author has declared that neither they nor their co-authors have any competing interests.

Disclaimer. Publisher's note: Copernicus Publications remains neutral with regard to jurisdictional claims in published maps and institutional affiliations.

Special issue statement. This article is part of the special issue "Simulation chambers as tools in atmospheric research (AMT/ACP/GMD inter-journal SI)". It is not associated with a conference.

Acknowledgements. The authors gratefully acknowledge support from the EU Horizon 2020 research and innovation programme through the EUROCHAMP-2020 Infrastructure Activity (grant agreement no. 730997) and the Deutsche Forschungsgemeinschaft (DFG) through the grant agreement WI 958/18-1. Rodrigo Gastón Gibilisco wish to acknowledges the Alexander von Humboldt Foundation for providing a Georg Forster Research Fellowship.

Financial support. This research has been supported by the Deutsche Forschungsgemeinschaft (grant no. WI 958/18-1) and the European Commission Horizon 2020 Framework Programme (grant no. EUROCHAMP-2020 (730997)).

Review statement. This paper was edited by Andreas Hofzumahaus and reviewed by two anonymous referees.

References

- Allen, G., Remedios, J. J., Newnham, D. A., Smith, K. M., and Monks, P. S.: Improved mid-infrared cross-sections for peroxyacetyl nitrate (PAN) vapour, *Atmos. Chem. Phys.*, 5, 47–56, <https://doi.org/10.5194/acp-5-47-2005>, 2005.
- Aschmann, S. M., Arey, J., and Atkinson, R.: Atmospheric Chemistry of Selected Hydroxycarbonyls, *J. Phys. Chem. A*, 104, 3998–4003, <https://doi.org/10.1021/jp9939874>, 2000.
- Atkinson, R.: Kinetics and Mechanisms of the Gas-Phase Reactions of the NO_3 Radical with Organic Compounds, *J. Phys. Chem. Ref. Data*, 20, 459–507, <https://doi.org/10.1063/1.555887>, 1991.
- Atkinson, R.: Rate constants for the atmospheric reactions of alkoxy radicals: An updated estimation method, *Atmos. Environ.*, 41, 8468–8485, <https://doi.org/10.1016/j.atmosenv.2007.07.002>, 2007.
- Atkinson, R., Baulch, D. L., Cox, R. A., Crowley, J. N., Hampson, R. F., Hynes, R. G., Jenkin, M. E., Rossi, M. J., Troe, J., and IUPAC Subcommittee: Evaluated kinetic and photochemical data for atmospheric chemistry: Volume II – gas phase reactions of organic species, *Atmos. Chem. Phys.*, 6, 3625–4055, <https://doi.org/10.5194/acp-6-3625-2006>, 2006.
- Barnes, I., Becker, K. H., and Zhu, T.: Near UV Absorption Spectra and Photolysis Products of Difunctional Organic Nitrates: Possible Importance as NO_x Reservoirs, *J. Atmos. Chem.*, 17, 353–373, <https://doi.org/10.1007/BF00696854>, 1993.

- Barnes, I., Becker, K. H., and Mihalopoulos, N.: An FTIR Product Study of the Photooxidation of Dimethyl Disulfide, *J. Atmos. Chem.*, 18, 267–289, <https://doi.org/10.1007/BF00696783>, 1994.
- Bickers, D. R., Calow, P., Greim, H. A., Hanifin, J. M., Rogers, A. E., Saurat, J.-H., Sipes, I. G., Smith, R. L., and Tagami, H.: The safety assessment of fragrance materials, *Regul. Toxicol. Pharm.*, 37, 218–273, [https://doi.org/10.1016/S0273-2300\(03\)00003-5](https://doi.org/10.1016/S0273-2300(03)00003-5), 2003.
- Blanco, M. B., Barnes, I., and Wiesen, P.: Kinetic Investigation of the OH Radical and Cl Atom Initiated Degradation of Unsaturated Ketones at Atmospheric Pressure and 298 K, *J. Phys. Chem. A*, 116, 6033–6040, <https://doi.org/10.1021/jp2109972>, 2012.
- Bloss, W. J., Evans, M. J., Lee, J. D., Sommariva, R., Heard, D. E., and Piling, M. J.: The oxidative capacity of the troposphere: Coupling of field measurements of OH and a global chemistry transport model, *Faraday Discuss.*, 130, 425–436, <https://doi.org/10.1039/B419090D>, 2005.
- Calvert, J. G., Atkinson, R., Kerr, J. A., Madronich, S., Moortgat, G. K., Wallington, T. J., and Yarwood, G.: The mechanisms of atmospheric oxidation of the alkenes, Oxford University Press, New York, 2000.
- Calvert, J. G., Mellouki, A., Orlando, J. J., Pilling, M. J., and Wallington, T. J.: The mechanisms of atmospheric oxidation of the oxygenates, Oxford University Press, New York, 2011.
- Calvert, J. G., Orlando, J. J., Stockwell, W. R., and Wallington, T. J.: The Mechanisms of Reactions Influencing Atmospheric Ozone, Oxford University Press, New York, 2015.
- Canosa-Mas, C. E., Flugge, M. L., King, M. D., and Wayne, R. P.: An experimental study of the gas-phase reaction of the NO₃ radical with α,β -unsaturated carbonyl compounds, *Phys. Chem. Chem. Phys.*, 7, 643–650, <https://doi.org/10.1039/B416574H>, 2005.
- Carrasco, N., Doussin, J.-F., Picquet-Varrault, B., and Carlier, P.: Tropospheric degradation of 2-hydroxy-2-methylpropanal, a photo-oxidation product of 2-methyl-3-buten-2-ol: Kinetic and mechanistic study of its photolysis and its reaction with OH radicals, *Atmos. Environ.*, 40, 2011–2019, <https://doi.org/10.1016/j.atmosenv.2005.11.042>, 2006.
- Carrasco, N., Doussin, J. F., O'Connor, M., Wenger, J. C., Picquet-Varrault, B., Durand-Jolibois, R., and Carlier, P.: Simulation Chamber Studies of the Atmospheric Oxidation of 2-Methyl-3-buten-2-ol: Reaction with Hydroxyl Radicals and Ozone Under a Variety of Conditions, *J. Atmos. Chem.*, 56, 33–55, <https://doi.org/10.1007/s10874-006-9041-y>, 2007.
- Chapuis, C. and Jacoby, D.: Catalysis in the preparation of fragrances and flavours, *Appl. Catal. A-Gen.*, 221, 93–117, [https://doi.org/10.1016/S0926-860X\(01\)00798-0](https://doi.org/10.1016/S0926-860X(01)00798-0), 2001.
- Etzkorn, T., Klotz, B., Sørensen, S., Patroescu, I. V., Barnes, I., Becker, K. H., and Platt, U.: Gas-phase absorption cross sections of 24 monocyclic hydrocarbons in the UV and IR spectral ranges, *Atmos. Environ.*, 33, 525–540, [https://doi.org/10.1016/S1352-2310\(98\)00289-1](https://doi.org/10.1016/S1352-2310(98)00289-1), 1999.
- Ezell, M. J., Wang, W., Ezell, A. A., Soskin, G., and Finlayson-Pitts, B. J.: Kinetics of reactions of chlorine atoms with a series of alkenes at 1 atm and 298 K: structure and reactivity, *Phys. Chem. Chem. Phys.*, 4, 5813–5820, <https://doi.org/10.1039/B207529F>, 2002.
- Fischer, E. V., Jacob, D. J., Yantosca, R. M., Sulprizio, M. P., Millet, D. B., Mao, J., Paulot, F., Singh, H. B., Roiger, A., Ries, L., Talbot, R. W., Dzepina, K., and Pandey Deolal, S.: Atmospheric peroxyacetyl nitrate (PAN): a global budget and source attribution, *Atmos. Chem. Phys.*, 14, 2679–2698, <https://doi.org/10.5194/acp-14-2679-2014>, 2014.
- Frost, M. J. and Smith, I. W. M.: Rate Constants for the Reactions of CH₃O and C₂H₅O with NO₂ over a Range of Temperature and Total Pressure, *J. Chem. Soc. Faraday T.*, 86, 1751–1756, <https://doi.org/10.1039/FT9908601751>, 1990.
- Fu, T.-M., Jacob, D. J., Wittrock, F., Burrows, J. P., Vrekoussis, M., and Henze, D. K.: Global budgets of atmospheric glyoxal and methylglyoxal, and implications for formation of secondary organic aerosols, *J. Geophys. Res. Atmos.*, 113, 1–17, <https://doi.org/10.1029/2007JD009505>, 2008.
- Fuchs, H., Albrecht, S., Acir, I., Bohn, B., Breitenlechner, M., Dorn, H.-P., Gkatzelis, G. I., Hofzumahaus, A., Holland, F., Kaminski, M., Keutsch, F. N., Novelli, A., Reimer, D., Rohrer, F., Tillmann, R., Vereecken, L., Wegener, R., Zaytsev, A., Kiendler-Scharr, A., and Wahner, A.: Investigation of the oxidation of methyl vinyl ketone (MVK) by OH radicals in the atmospheric simulation chamber SAPHIR, *Atmos. Chem. Phys.*, 18, 8001–8016, <https://doi.org/10.5194/acp-18-8001-2018>, 2018.
- Galloway, M. M., Huisman, A. J., Yee, L. D., Chan, A. W. H., Loza, C. L., Seinfeld, J. H., and Keutsch, F. N.: Yields of oxidized volatile organic compounds during the OH radical initiated oxidation of isoprene, methyl vinyl ketone, and methacrolein under high-NO_x conditions, *Atmos. Chem. Phys.*, 11, 10779–10790, <https://doi.org/10.5194/acp-11-10779-2011>, 2011.
- Gaona-Colmán, E., Blanco, M. B., and Teruel, M. A.: Kinetics and product identification of the reactions of (*E*)-2-hexenyl acetate and 4-methyl-3-penten-2-one with OH radicals and Cl atoms at 298 K and atmospheric pressure, *Atmos. Environ.*, 161, 155–166, <https://doi.org/10.1016/j.atmosenv.2017.04.033>, 2017.
- Gratien, A., Nilsson, E., Doussin, J.-F., Johnson, M. S., Nielsen, C. J., Stenström, Y., and Picquet-Varrault, B.: UV and IR Absorption Cross-sections of HCHO, HCDO, and DCDO, *J. Phys. Chem. A*, 111, 11506–11513, <https://doi.org/10.1021/jp074288r>, 2007.
- Green, M., Yarwood, G., and Niki, H.: FTIR Study of the Cl-Atom Initiated Oxidation of Methylglyoxal, *Int. J. Chem. Kinet.*, 22, 689–699, <https://doi.org/10.1002/kin.550220705>, 1990.
- Grosjean, D. and Williams II, E. L.: Environmental persistence of organic compounds estimated from structure-reactivity and linear free-energy relationships. Unsaturated Aliphatics, *Atmos. Environ. A-Gen.*, 26, 1395–1405, [https://doi.org/10.1016/0960-1686\(92\)90124-4](https://doi.org/10.1016/0960-1686(92)90124-4), 1992.
- Guenther, A., Karl, T., Harley, P., Wiedinmyer, C., Palmer, P. I., and Geron, C.: Estimates of global terrestrial isoprene emissions using MEGAN (Model of Emissions of Gases and Aerosols from Nature), *Atmos. Chem. Phys.*, 6, 3181–3210, <https://doi.org/10.5194/acp-6-3181-2006>, 2006.
- Hatch, L. E., Yokelson, R. J., Stockwell, C. E., Veres, P. R., Simpson, I. J., Blake, D. R., Orlando, J. J., and Barsanti, K. C.: Multi-instrument comparison and compilation of non-methane organic gas emissions from biomass burning and implications for smoke-derived secondary organic aerosol precursors, *Atmos. Chem. Phys.*, 17, 1471–1489, <https://doi.org/10.5194/acp-17-1471-2017>, 2017.

- Illmann, J. N., Patroescu-Klotz, I., and Wiesen, P.: Gas-phase reactivity of acyclic α,β -unsaturated carbonyls towards ozone, *Phys. Chem. Chem. Phys.*, 23, 3455–3466, <https://doi.org/10.1039/D0CP05881E>, 2021a.
- Illmann, N., Patroescu-Klotz, I., and Wiesen, P.: Biomass burning plume chemistry: OH radical initiated oxidation of 3-penten-2-one and its main oxidation product 2-hydroxypropanal, *Atmos. Chem. Phys. Discuss.* [preprint], <https://doi.org/10.5194/acp-2021-575>, in review, 2021b.
- Jenkin, M. E., Valorso, R., Aumont, B., Rickard, A. R., and Wallington, T. J.: Estimation of rate coefficients and branching ratios for gas-phase reactions of OH with aliphatic organic compounds for use in automated mechanism construction, *Atmos. Chem. Phys.*, 18, 9297–9328, <https://doi.org/10.5194/acp-18-9297-2018>, 2018.
- Kanakidou, M., Seinfeld, J. H., Pandis, S. N., Barnes, I., Dentener, F. J., Facchini, M. C., Van Dingenen, R., Ervens, B., Nenes, A., Nielsen, C. J., Swietlicki, E., Putaud, J. P., Balkanski, Y., Fuzzi, S., Horth, J., Moortgat, G. K., Winterhalter, R., Myhre, C. E. L., Tsigaridis, K., Vignati, E., Stephanou, E. G., and Wilson, J.: Organic aerosol and global climate modelling: a review, *Atmos. Chem. Phys.*, 5, 1053–1123, <https://doi.org/10.5194/acp-5-1053-2005>, 2005.
- Kwok, E. S. C. and Atkinson, R.: Estimation of hydroxyl radical reaction rate constants for gas-phase organic compounds using a structure-reactivity relationship: An update, *Atmos. Environ.*, 29, 1685–1695, [https://doi.org/10.1016/1352-2310\(95\)00069-B](https://doi.org/10.1016/1352-2310(95)00069-B), 1995.
- Li, W., Dan, G., Chen, M., Wang, Z., Zhao, Y., Wang, F., Li, F., Tong, S., and Ge, M.: The gas-phase reaction kinetics of different structure of unsaturated alcohols and ketones with O_3 , *Atmos. Environ.*, 254, 118394, <https://doi.org/10.1016/j.atmosenv.2021.118394>, 2021.
- Logan, J. A.: Tropospheric Ozone: Seasonal Behavior, Trends, and Anthropogenic Influence, *J. Geophys. Res.*, 90, 10463–10482, <https://doi.org/10.1029/JD090iD06p10463>, 1985.
- Matsunaga, A. and Ziemann, P. J.: Yields of β -hydroxynitrates, dihydroxynitrates, and trihydroxynitrates formed from OH radical-initiated reactions of 2-methyl-1-alkenes, *P. Natl. Acad. Sci. USA*, 107, 6664–6669, <https://doi.org/10.1073/pnas.0910585107>, 2010.
- Mellouki, A., Wallington, T. J., and Chen, J.: Atmospheric Chemistry of Oxygenated Volatile Organic Compounds: Impacts on Air Quality and Climate, *Chem. Rev.*, 115, 3984–4014, <https://doi.org/10.1021/cr500549n>, 2015.
- Mellouki, A., Ammann, M., Cox, R. A., Crowley, J. N., Herrmann, H., Jenkin, M. E., McNeill, V. F., Troe, J., and Wallington, T. J.: Evaluated kinetic and photochemical data for atmospheric chemistry: volume VIII – gas-phase reactions of organic species with four, or more, carbon atoms ($\geq C_4$), *Atmos. Chem. Phys.*, 21, 4797–4808, <https://doi.org/10.5194/acp-21-4797-2021>, 2021.
- Mund, C., Fockenberg, C., and Zellner, R.: LIF Spectra of *n*-Propoxy Radicals and Kinetics of their Reactions with O_2 and NO_2 , *Ber. Bunsenges. Phys. Chem.*, 102, 709–715, <https://doi.org/10.1002/bbpc.19981020502>, 1998.
- Nakanaga, T., Kondo, S., and Saeki, S.: Infrared band intensities of formaldehyde and formaldehyde- d_2 , *J. Chem. Phys.*, 76, 3860–3865, <https://doi.org/10.1063/1.443527>, 1982.
- Noda, J., Hallquist, M., Langer, S., and Ljungström, E.: Products from the gas-phase reaction of some unsaturated alcohols with nitrate radicals, *Phys. Chem. Chem. Phys.*, 2, 2555–2564, <https://doi.org/10.1039/B000251H>, 2000.
- Notario, A., Le Bras, G., and Mellouki, A.: Absolute Rate Constants for the Reactions of Cl Atoms with a Series of Esters, *J. Phys. Chem. A*, 102, 3112–3117, <https://doi.org/10.1021/jp980416n>, 1998.
- Orlando, J. J., Tyndall, G. S., Vereecken, L., and Peeters, J.: The Atmospheric Chemistry of the Acetonyl Radical, *J. Phys. Chem. A*, 104, 11578–11588, <https://doi.org/10.1021/jp0026991>, 2000.
- Orlando, J. J., Tyndall, G. S., and Wallington, T. J.: The Atmospheric Chemistry of Alkoxy Radicals, *Chem. Rev.*, 103, 4657–4689, <https://doi.org/10.1021/cr020527p>, 2003.
- Paulot, F., Crouse, J. D., Kjaergaard, H. G., Kroll, J. H., Seinfeld, J. H., and Wennberg, P. O.: Isoprene photooxidation: new insights into the production of acids and organic nitrates, *Atmos. Chem. Phys.*, 9, 1479–1501, <https://doi.org/10.5194/acp-9-1479-2009>, 2009.
- Picquet-Varrault, B., Doussin, J.-F., Durand-Jolibois, R., Pirali, O., and Carlier, P.: Kinetic and Mechanistic Study of the Atmospheric Oxidation by OH Radicals of Allyl Acetate, *Environ. Sci. Technol.*, 36, 4081–4086, <https://doi.org/10.1021/es0200138>, 2002.
- Picquet-Varrault, B., Suarez-Bertoa, R., Duncianu, M., Cazaunau, M., Pangui, E., David, M., and Doussin, J.-F.: Photolysis and oxidation by OH radicals of two carbonyl nitrates: 4-nitrooxy-2-butanone and 5-nitrooxy-2-pentanone, *Atmos. Chem. Phys.*, 20, 487–498, <https://doi.org/10.5194/acp-20-487-2020>, 2020.
- Praske, E., Crouse, J. D., Bates, K. H., Kurtén, T., Kjaergaard, H. G., and Wennberg, P. O.: Atmospheric Fate of Methyl Vinyl Ketone: Peroxy Radical Reactions with NO and HO_2 , *J. Phys. Chem. A*, 119, 4562–4572, <https://doi.org/10.1021/jp5107058>, 2015.
- Profeta, L. T. M., Sams, R. L., and Johnson, T. J.: Quantitative Infrared Intensity Studies of Vapor-Phase Glyoxal, Methylglyoxal, and 2,3-Butanedione (Diacyl), with Vibrational Assignments, *J. Phys. Chem. A*, 115, 9886–9900, <https://doi.org/10.1021/jp204532x>, 2011.
- Sato, K., Klotz, B., Taketsuga, T., and Takayagi, T.: Kinetic measurements for the reactions of ozone with crotonaldehyde and its methyl derivatives and calculations of transition-state theory, *Phys. Chem. Chem. Phys.*, 6, 3696–3976, <https://doi.org/10.1039/B402496F>, 2004.
- Siegel, H. and Eggersdorfer, M.: Ketones, *Ullmann's Encyclopedia of Industrial Chemistry*, Wiley-VCH Verlag, Weinheim, https://doi.org/10.1002/14356007.a15_077, 2000.
- Sifniades, S., Levy, A. B., and Bahl, H.: Acetone, *Ullmann's Encyclopedia of Industrial Chemistry*, Wiley-VCH Verlag, Weinheim, https://doi.org/10.1002/14356007.a01_079.pub3, 2011.
- Smith, I. W. M. and Ravishankara, A. R.: Role of Hydrogen-Bonded Intermediates in the Bimolecular Reactions of the Hydroxyl Radical, *J. Phys. Chem. A*, 106, 4798–4807, <https://doi.org/10.1021/jp014234w>, 2002.
- Spittler, M.: Untersuchungen zur troposphärischen Oxidation von Limonen: Produktanalysen, Aerosolbildung und Photolyse von Produkten, PhD thesis, Bergische Universität Wuppertal, Germany, 2001.

- Suarez-Bertoa, R., Picquet-Varrault, B., Tamas, W., Pangui, E., and Doussin, J.-F.: Atmospheric Fate of a Series of Carbonyl Nitrates: Photolysis Frequencies and OH-Oxidation Rate Constants, *Environ. Sci. Technol.*, 46, 12502–12509, <https://doi.org/10.1021/es302613x>, 2012.
- Talukdar, R. K., Zhu, L., Feierabend, K. J., and Burkholder, J. B.: Rate coefficients for the reaction of methylglyoxal (CH_3COCHO) with OH and NO_3 and glyoxal (HCO)₂ with NO_3 , *Atmos. Chem. Phys.*, 11, 10837–10851, <https://doi.org/10.5194/acp-11-10837-2011>, 2011.
- Taylor, W. D., Allston, T. D., Moscato, M. J., Fazekas, G. B., Kozlowski, R., and Takacs, G. A.: Atmospheric photodissociation lifetimes for nitromethane, methyl nitrite, and methyl nitrate, *Int. J. Chem. Kinet.*, 12, 231–240, <https://doi.org/10.1002/kin.550120404>, 1980.
- Tuazon, E. C. and Atkinson, R.: A Product Study of the Gas-Phase Reaction of Methyl Vinyl Ketone with the OH Radical in the Presence of NO_x , *Int. J. Chem. Kinet.*, 21, 1141–1152, <https://doi.org/10.1002/kin.550211207>, 1989.
- Tuazon, E. C., MacLeod, H., Atkinson, R., and Carter, W. P. L.: α -Dicarbonyl yields from the NO_x -air photooxidation of a series of aromatic hydrocarbons in air, *Environ. Sci. Technol.*, 20, 383–387, <https://doi.org/10.1021/es00146a010>, 1986.
- US EPA: Estimation Programs Interface Suite™ for Microsoft® Windows, v 4.11. United States Environmental Protection Agency, Washington, DC, USA, 2021.
- Vereecken, L. and Peeters, J.: Decomposition of substituted alkoxy radicals – part I: a generalized structure-activity relationship for reaction barrier heights, *Phys. Chem. Chem. Phys.*, 11, 9062–9074, <https://doi.org/10.1039/B909712K>, 2009.
- Vyskocil, A., Viau, C., and Lamy, S.: Peroxyacetyl nitrate: review of toxicity, *Hum. Exp. Toxicol.*, 17, 212–220, <https://doi.org/10.1177/096032719801700403>, 1998.
- Wang, J., Zhou, L., Wang, W., and Ge, M.: Gas-phase reaction of two unsaturated ketones with atomic Cl and O_3 : kinetics and products, *Phys. Chem. Chem. Phys.*, 17, 12000–12012, <https://doi.org/10.1039/C4CP05461J>, 2015.
- Wang, X., Hong, P., Kiss, A. A., Wang, Q., Li, L., Wang, H., and Qiu, T.: From Batch to Continuous Sustainable Production of 3-Methyl-3-penten-2-one for Synthetic Ketone Fragrances, *ACS Sustain. Chem. Eng.*, 8, 17201–17214, <https://doi.org/10.1021/acssuschemeng.0c05908>, 2020.
- Wingenter, O. W., Kubo, M. K., Blake, N. J., Smith Jr., T. W., Blake, D. R., and Rowland, F. S.: Hydrocarbon and halocarbon measurements as photochemical and dynamical indicators of atmospheric hydroxyl, atomic chlorine, and vertical mixing obtained during Lagrangian flights, *J. Geophys. Res.*, 101, 4331–4340, <https://doi.org/10.1029/95JD02457>, 1996.
- Winiberg, F. A. F., Dillon, T. J., Orr, S. C., Groß, C. B. M., Bejan, I., Brumby, C. A., Evans, M. J., Smith, S. C., Heard, D. E., and Seakins, P. W.: Direct measurements of OH and other product yields from the $\text{HO}_2 + \text{CH}_3\text{C}(\text{O})\text{O}_2$ reaction, *Atmos. Chem. Phys.*, 16, 4023–4042, <https://doi.org/10.5194/acp-16-4023-2016>, 2016.